The Plymouth Student Scientist - Volume 01 - 2008 The Plymouth Student Scientist - Volume 1, No. 1 - 2008

2008

Turbulent Mixing in Bottom Boundary Layer of the Coastal Ocean

Kaczmarska, A.

Kaczmarska, A. (2008) 'Turbulent Mixing in Bottom Boundary Layer of the Coastal Ocean', The Plymouth Student Scientist, 1(1), p. 162-228
http://hdl.handle.net/10026.1/12807

The Plymouth Student Scientist
University of Plymouth

*The Plymouth Student Scientist, 2008, **1,** (1), 162-228*

Turbulent Mixing in Bottom Boundary Layer of the Coastal Ocean

Anna Kaczmarska
2007

Project Advisor:,Alex Nimmo Smith School of Earth, Ocean & Environmental Sciences, University of Plymouth, Drake Circus, Plymouth, PL4 8AA

Abstract

This paper analyses the evolution of the bottom boundary layer observed over a flood tide in the Plymouth Sound in June 2006. The overview of the energy budget associated with turbulence is presented in which an estimation of turbulent energy dissipation and production in the boundary layer is performed. Turbulent characteristics are calculated from data collected by two Acoustic Doppler Velocimeters (ADV) located at 69 cm and 52 cm above the sea bed. The same turbulent characteristics are calculated, but applying different methods, using the velocity measured by a downlooking 1200 kHz Acoustics Doppler Current Profiler (ADCP) installed at a height 1.36m above the bed. The study compares turbulent characteristics calculated from data collected by two different types of instruments. Additionally, the currents in the whole water column are examined by analysing profiles of velocity collected by 600 kHz ADCP. The study checks whether the velocities measured by the two ADCPs are consistent with each other and examines the possible effects of density stratification on turbulence in the bottom boundary layer.

It was found that the flow was an effect of semidiurnal tide with the maximum velocities of 22cm/s observed two hours after Low Water 4m above the bed. Velocity profiles, measured by the two ADCP, did not overlap each other but the results are consistent with each other. Measurements performed by both ADVs showed the same magnitudes and trends in the mean velocity as the 1.2MHz ADCP. The results indicated weak stratification in the water column. Velocities measured by 1.2MHz ADCP had logarithmic profiles from which the friction velocity (u_*) and bed stress (τ_b) were calculated. The characteristics had similar values (u_*<1cm/s, τ_b<0.09Pa) as reported previously for similar conditions (flat bed, tidal channel, unstratified water column). Dissipation rate (ε) calculated from the two ADVs provided inaccurate results which were three orders of a magnitude higher than that obtained from the higher frequency ADCP (10^{-8}-10^{-6} W/kg). That difference was found to be associated with the assumptions of the first method, which were not fulfilled. The production of TKE (P), from ADVs and the 1.2MHz ADCP, had the same magnitude than ε and the average ε/P ratio, over the whole time of deployment, was found to be 1.45 +/- 1.07. However, the ratio was biased by the high ε during run 2. After rejecting that run the ratio was closer to the expected value of unity: 0.78 +/- 0.36.

ISSN 1754-2383 [Online]

Acknowledgments

A number of people have been important in the planning this research and writing the final paper. The initial idea was inspired by Dr Alex Nimmo Smith who provided the support during data collection and analysis. I am grateful for his support with programming in Matlab and interpretation of the results.

My acknowledgment goes to the people who helped making the measurements reported in this paper: Mr Peter Ganderton for an ADCP and an ADV technical support, Mr Tim Stevens for his assistance during CTD profiling and Dr Alex Nimmo Smith for organising the deployment.

CONTENTS PAGE

List of Figures

List of Tables

1.0 INTRODUCTION

Turbulent mixing and flow characteristics are essential elements in understanding coastal hydrodynamics and development of oceanographic models. Bottom generated turbulence is a key factor for understanding sedimentation and resuspension of bottom material (Dyer, 1997). Understanding turbulence will make possible prediction of the distribution of the pollutants, nutrients and planktonic organisms in the ocean (Stainsen & Sunby, 2001; Rothschild & Osborn, 1988).

Turbulence is important because it promotes mixing and dispersion in the fluid by eddy diffusion of heat, salt and mass. However, in the ocean, the structure of turbulence varies in time and space (location) though its velocity scale is defined. In coastal regions, distribution of turbulence and circulation vary in position, depending on tidal amplitude, river flow and meteorological conditions (Sylaiosa and Boxall, 1998). Mixing processes also change in time due to the tidal cycle and can cause a series of stratification and destratification in the water column. All of the above processes cause the turbulence distribution to become complex and difficult to measure. Because of that it is still not known how or why turbulence occurs and predicting turbulent behaviour with any degree of reliability, even in very simple flow situations is difficult (McDonough, 2004). Therefore further study is needed to understand turbulence and the associated energy budget and mass transport.

Over recent years, the ability to measure dissipation and production of turbulent kinetic energy (TKE) has increased with development of new techniques such as:
Particle Tracking Velocimetry, high frequency Acoustic Doppler Current Profilers (ADCP), Laser and Acoustic Doppler Velocimeters (ADV). This has led to major advances in understanding of turbulent processes. Measurements of Reynolds stress and turbulent parameters near the sea bed have been recently made using ADV (Kim et al., 2000) and a high frequency ADCP (Garret, 1999, Lorke & Wuest, 2005). Novel methods have been proposed for estimation of turbulent characteristics that make the calculation much quicker.

The estimation of turbulent dissipation rate from ADCP has also been developed recently (Wiles et al., 2006).This study applies this novel technique to calculate the dissipation rate from ADCP velocity data over a flood tide. The results will be

compared to the dissipation rate obtained using the Kolmogorov's spectral method on ADV data. Furthermore, the production of turbulent kinetic energy (TKE) will be estimated directly from ADV velocity measurements and by applying the 'variance method' (Lohrmann et al., 1990, Stacey et al. 1999) on the data collected by a downward looking 1.2MHz ADCP attached to a bed frame at a height of 1.36m above the bottom.

In summary, this research tries to answer the following questions:

- Is the flow in the bottom boundary layer (BBL) fully turbulent?
- What is the shape of the BBL and how it changes with time during the flood tide?
- Is the flow in the equilibrium: Is the production of TKE balanced by the dissipation?
- What is the order of stratification during the deployment and does it affect turbulence in BBL?
- Are turbulent characteristics, obtained using different methods, consistent with each other?
- Are the results consistent with the results obtained by other studies performed in similar environment (flat plate, channel, tidal flow)?

The next chapter contains the theory of turbulence. It provides background information about turbulent characteristics, turbulent bottom boundary layer and turbulent kinetic energy balance occurring in the flow. Furthermore, it describes the theory behind various techniques used in this study for the calculation of turbulent production and dissipation rate. Chapter 3 describes data collection and analysis. It also provides the information about principles of operation and instruments settings used during the measurements. The results are presented and discussed in chapter 4. Firstly, the general background about the flow structure and stratification is reported. Afterwards, time series of turbulent dissipation and production obtained from ADV and ADCP are compared, and subsequently contrasted with previous studies. Finally, chapter 5 contains a summary and conclusions of the report.

2.0 THEORY

2.1 What is turbulence, and when it occurs?

Most of the flows occurring in nature are turbulent (McDonough, 2004). Turbulence is a manifestation of the flow and originates in the instability of shear flows. It can be characterised by a rotational three-dimensional motion, which generates large gradients of velocity at the small scales and therefore promotes dissipation of kinetic energy into heat. This makes turbulence a highly dissipative process and therefore a source of energy must be present to maintain the process.

In 1883 Osborne Reynolds published the first paper, which described the transition from laminar to turbulent flow. He concluded that the transition occurs at higher speeds, when Reynolds number (R_e), which determines resistance to the flow, exceeds $1.3*10^4$ (R_e= UD/*v* where U is an average velocity in the water column, D is a stream distance, *v* is a kinematic viscosity) (McDonough, 2004). The transition could be explained by the Navier-Stokes equation, from which can be deduced that the nonlinear convective terms become important at high Reynolds numbers.

Different studies showed that the critical value of Reynolds number increases when the disturbances in the flow decrease. It was confirmed by laboratory experiments that the flow can be still laminar at critical R_e of about 40 000 by providing the flow was free of disturbances (Ekman in Schlichting, 1968). Therefore, it is not easy to estimate when the flow becomes turbulent because the amplitude and type of perturbations must be also considered (Mathieu & Scott, 2000). More recently, the investigations of the transition process showed that in a certain range around the critical Reynolds number, the flow alternates between laminar and turbulent (Schlichting, 1968).

In coastal boundary layers the transition from laminar to turbulent flow is affected by mean parameters: pressure distribution in the external flow, roughness of the sea bed and the nature of disturbances. The presence of bed roughness favours the transition by decreasing the critical value of the Reynolds number. The existence of irregularities on the sea bed give rise to additional disturbances in the flow and, in a consequence, a lower degree of amplification is sufficient to effect a transition from laminar to turbulent flow. Another important parameter on the stability of the flow is density variation. When the flow has density stratification, turbulent mixing can be

strongly affected. This is true especially in the vertical direction where the parcels of fluid must be moved against hydrostatic forces. Richardson, in 1926, has shown that the stability of the flow is proportional to the gradient of density and the vertical gradient of velocity magnitude:

$$Ri = -\frac{g}{\rho}\frac{\frac{\partial \rho}{\partial z}}{\left(\frac{\partial u}{\partial z}\right)^2 + \left(\frac{\partial v}{\partial z}\right)^2} \qquad (1)$$

where *Ri* is the Richardson number, g is the gravitational acceleration, ρ is the density of the fluid, u, v are the horizontal velocity components and z is the vertical distance.

The experiments performed later by L. Prandl (1929) revealed that turbulence may be completely suppressed at Richardson number equal to two (Schilchting, 1968). Taylor (1931) re-examined Prandl's results and obtained the Richardson number equal to one as a limit of stability in the flow.

2.2 Turbulent bottom boundary layer

At the bottom of the ocean the water flowing above the sea bed causes stress which extends throughout the water column. Near the bed, the velocity decreases due to the friction. The part of the flow where the velocity is affected by the bed is called the boundary layer. In the laminar boundary layer the velocity shear (du/dz) increases linearly with increase in shear stress (τ_v):

$$\tau_v = \mu \frac{du}{dz} \quad (2)$$

where μ is the dynamic viscosity.

At sufficiently high Reynolds number the flow in the boundary layer becomes turbulent due to instability present in the flow. As a consequence the flow develops a highly random character with rapid irregular fluctuations of velocity in space and in time. The velocity at any point in space (u) can be described by its time average (U) and fluctuating part (u'): u=U+u'. It can be noticed that the fluctuating parts of velocity vector give rise to an additional stresses in the flow, called Reynolds stresses which increase with distance from the boundary together with the intensity of turbulence. Therefore, a total shear stress in the turbulent bottom boundary layer is a product of viscous and Reynolds stress. It varies with height above the bed, but near the bed, reaches the constant value defined as the bed shear stress (τ_b). This parameter makes possible to define a shear velocity (u_*) that represents the strength of turbulent velocity fluctuations near the bed: $u_* = \sqrt{\frac{\tau_b}{\rho}}$ and $u_* \approx \sqrt{(\overline{u'w'})}$. For relatively smooth bottoms the friction velocity was found to be around 0.2cm/s for flat bottoms (Chris and Cadwell, 1984), 1cm/s when a surface swell occurred (Grant et al.,1984), and few cm/s when bottom roughness was present (Cacchione et al., 1994).

In the turbulent boundary layer, close to the bottom, the size of the largest scales of turbulent eddies decreases and becomes the same as the smallest scales. Close to the wall, the velocity fluctuations are damped and the viscous stresses dominate. The layer where this is true is called a viscous (or laminar) boundary layer which exists where the transition between the flow and bottom sediments occurs (Figure 1). Here, viscous and turbulent momentum transfer across the flow are important and viscous stress cannot be neglected. The velocity profile in the layer is almost linear,

increasing from zero at the sea bed. The thickness of this region (∂_v) is approximately $\partial_v = 11.6v/u_*$ and for the coastal ocean reaches several millimetres.

Above the viscous sublayer there is a transition layer where the viscous and Reynolds stress have similar magnitude. The transition occurs to a region where the mean velocity of the flow varies as the natural logarithm of height above the bed (z) (Figure 1):

$$u(z) = \frac{u_*}{k} \ln\left[\frac{z}{z_0}\right] \qquad (3)$$

where k is a Von Karman's constant equal to 0.41 and z_0 is a bed roughness.

The region in which equation (3) applies is called the logarithmic layer or a log-layer. The relationship was obtained assuming a constant bed shear stress and it is valid for steady and uniform flows. The stress in the region changes linearly $\tau \approx \tau_b(1 - z/h)$ and the region it occupies depends on water depth and flow velocity. The above relationship is often used to estimate a stress and roughness from the measurements of velocity profiles by fitting a straight line to u(z) versus ln(z). The equation of the line y=ax+b makes possible to calculate u_* and z_0 from the slope $a=u_*/k$ and the intercept $b=a*\ln(z_0)$.

In the logarithmic layer the momentum is transferred mostly via the Reynolds stress. The viscosity is still responsible for the dissipation but turbulent momentum transfer dominates in the flow. Because turbulent momentum transfer in the logarithmic layer is much more efficient than viscous diffusion, turbulent boundary layers are thicker and have higher skin friction than laminar boundary layers. There are several processes that may cause the boundary layer shape to become non-logarithmic. For example, surface waves and density stratification can affect bottom boundary layer shape (Grant et al., 1984). It was found that the log layer forms only when the mean flow is faster than the orbital motion caused by waves (Nimmo Smith et al. 2001). Additionally, acceleration or deceleration of the flow, bottom roughness and suspended sediments modify the shape of BBL(Cacchione & Drake, 1990).

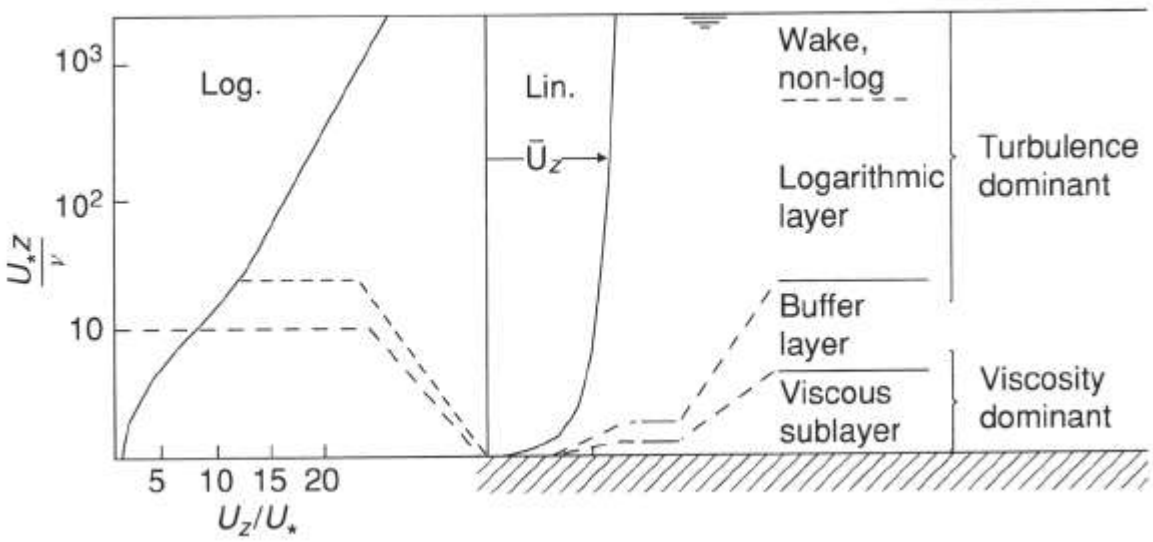

Figure 1. *Regions of the turbulent boundary layer. A typical velocity distribution across the whole of the turbulent boundary layer is shown when the x axis is logarithmic (Log.) and linear (Lin.)(source :McCave, 2005).*

2.3 Turbulent Kinetic energy (TKE) budget

Osborne Reynolds first recognised that an essential feature of turbulence is that turbulent eddies transfer momentum (heat and salinity) across fixed surfaces (Mathieu & Scott, 2000). Kinetic energy in the turbulent flow is produced by shear and buoyancy and destroyed by dissipation. It can be also transported into (gain) or out (loss) of the considered region. To understand how turbulence varies with time a turbulent kinetic energy budget must be quantified.

The turbulent kinetic energy (TKE) equation represents transfer of turbulent kinetic energy between the mean flow and turbulence (Equation 4). Here, a boundary layer approximation was applied to a steady and two-dimensional flow. Equation 4 is presented in tensor notation: i,j,k=1,2,3, and i=j (two dimensions).

.

$$\frac{1}{2}\overline{U}_k \frac{\partial\left(\overline{q^2}\right)}{\partial x_k} = -\overline{u_i u_k}\frac{\partial \overline{U}_i}{\partial x_k} - \frac{1}{2}\frac{\partial \overline{q^2 u_k}}{\partial x_k} - \frac{1}{\rho}\overline{u_i \frac{\partial p}{\partial x_i}} + \nu \overline{u_i \frac{\partial^2 u_i}{\partial^2 x_k}} \quad (4)$$

where:

$\overline{q^2} = 3u'^2 = \overline{u_i u_i}$ - Total, mean squared turbulent velocity,

A) $\frac{1}{2}\overline{U}_k \frac{\partial\left(\overline{q^2}\right)}{\partial x_k}$ - Convection of turbulent energy by the mean flow.

B) $-\overline{u_i u_k}\frac{\partial \overline{U}_i}{\partial x_k}$ - Production of turbulent energy by interaction between the mean flow and turbulence,

C) $-\frac{1}{2}\frac{\partial \overline{q^2 u_k}}{\partial x_k}$ -Advective transport of turbulent energy by fluctuating motion (turbulent mixing)

D) $-\frac{1}{\rho}\overline{u_i \frac{\partial p}{\partial x_i}}$ -Transfer of turbulent energy by pressure effects (work done by fluctuating pressure),

E) $\nu \overline{u_i \frac{\partial^2 u_i}{\partial^2 x_j}}$ - Viscous dissipation and diffusion,

Term A) is a rate of change of turbulent energy per unit mass, which is equal to the sum of other terms: B+C+D+E. It describes a convection of turbulent energy by the mean flow. The production of turbulence is described by term B). It can be interpreted as representing TKE production, which can be understood as the amount of energy transferred from the mean flow to turbulence. Equation 4 shows that without mean velocity gradients there is no production in the flow. In such a case,

turbulent energy is dissipated and decreases continuously. The regions of high turbulence production are associated with the locations of maximum mean shear, which occur near the wall for the channel flow.

The production term depends also on Reynolds stress tensor (u_iu_j) that represents the average momentum flux due to turbulent velocity fluctuations. The Reynolds stress is equal to zero for homogenous turbulence and in consequence has no effect on the mean flow (Mathieu & Scott, 2000). When the turbulence is equal in all directions (isotropic) the tensor is diagonal and all its diagonal elements are equal. In the channel Reynolds stress was found to be negative for events generated at the sea bed and positive for events generated at the sea surface (Mathieu &Scot,2000). Therefore, turbulent eddies coming from opposite vertical directions tend to cancel each other in the centre of the channel.

The last term of the equation 4, the viscous dissipation and diffusion, can be rewritten as:

$$\overline{\nu u_i \frac{\partial^2 u_i}{\partial^2 x_k}} = \nu \frac{\partial}{\partial x_j}\left[\overline{u_i\left(\frac{\partial u_i}{\partial x_j}+\frac{\partial}{\partial x_i}\right)}\right] - \bar{\varepsilon} \qquad (5)$$

viscous transfer — dissipation of turbulent energy

where the rate of energy dissipation is defined as : $\bar{\varepsilon} = \frac{1}{2}\nu\overline{\left(\frac{\partial u_i}{\partial x_j}+\frac{\partial u_j}{\partial x_i}\right)\left(\frac{\partial u_i}{\partial u_j}+\frac{\partial u_j}{\partial u_i}\right)}$

and can be interpreted as the average turbulent energy dissipation rate. The viscous transfer term is very small at high Reynolds number and can be neglected, except in the viscous sublayer. It integrates to zero over the whole flow and does not lead to any net changes in the TKE.

The dissipation rate is a very important parameter and cannot be neglected when considering the turbulence energy balance. This term is always positive and it is controlled by the largest scales of eddies (energy suppliers). Therefore the dissipation rate together with viscosity determines the velocity gradients and size of dissipative scales. At high enough Reynolds numbers, turbulent energy dissipates due to an energy cascade from larger to smaller eddies (Bradshaw, 1971). Firstly, the kinetic energy is transferred from the mean flow and large scale eddies are formed. The large eddies continuously supply the energy to the small eddies, which

then transfer it to even smaller eddies and so on. The energy is then dissipated into heat by the smallest scales of turbulent eddies. The convection by the mean flow and diffusion are equal to zero when integrated over the whole flow. Furthermore, the transfer terms are zero for homogenous turbulence. Therefore, for homogenous turbulence, TKE changes only due to the production and dissipation. Moreover, when the flow does not change in time (is steady) there is a balance between the production and dissipation of turbulent energy.

However, some variation with height in the turbulent boundary layer exists even when there is a balance between production and dissipation of TKE. Laufer (1954) reported for a pipe (similar case to a channel) that production and dissipation rise when approaching the boundary. He found that the maximum production occurs close to the wall in the viscous sub-layer. Therefore most of turbulence is generated in the viscous sub-layer but some of it is dissipated there. The dissipation was found to have a maximum in the central part of the flow, when the shear is lower. Furthermore, the above study found that turbulence is anisotropic and inhomogeneous in vertical direction.

2.4 Techniques applied to calculate turbulent characteristics

2.4.1 Calculation of Dissipation rate using ADV velocity measurements

If the flow is fully turbulent (high Reynolds number), the mean square velocity increases between two points, separated by some distance, is proportional to the power of two-thirds of the distance (Kolmogorov, 1941). The same scaling should hold for the velocity components. The law is called '2/3 law' and holds in the inertial subrange (Figure 2) of the energy spectrum corresponding to Taylor microscales. It is possible to derive TKE spectrum using a dimensional analysis. Tennekes (1975) derived from the Kolomogrov's law that turbulent energy of the frequency spectrum can be explained by:

$$S(\omega) = B\varepsilon^{2/3} u_{rms}{}^{2/3} \omega^{-5/3} \quad (6)$$

where *S(ω)* is the spectral density at angular frequency *ω*, *B* is a non-dimensional constant assumed to be of order of one (Tennekes & Lumley, 1974); *ε* is the energy dissipation rate and u_{rms} is the root-mean square of the fluctuating part of the velocity (u').

Stainsen & Sunby (2000) showed that the spectrum can be expressed in terms of the natural frequency $f=\omega/2\pi$:

$$S(f) = C_f \varepsilon^{2/3} u_{rms}{}^{2/3} f^{-5/3} \quad (7)$$

where $C_f = B(2\pi)^{-2/3}$.

The above relationship holds for the inertial subrange (See figure 2) when the turbulent flow is stationary, homogenous and isotropic. The inertial range is the range of length scales (or wavenumbers) in which viscous effects are negligible. In terms of the energy spectrum (Figure 2), the inertial scale is often identified with the wavenumbers (or frequencies) corresponding to the maximum energy.

It is possible to fit a straight line in the inertial subrange in the log-log plot of S vs ω: $y = \log_{10}(S(\omega))$ and $x = \log_{10}(\omega)$. The result is:

$$S(\omega) = \omega^a \cdot 10^b$$

where *a* is the slope of the line equal to -5/3 from eq.4 and $10^b = B\varepsilon^{2/3} u_{rms}{}^{2/3}$ is the intercept of the straight line y=ax+b.

Therefore, it is possible to calculate dissipation rate for natural frequency (Stainsen & Sunby, 2000):

$$\varepsilon = 2\pi\left(\frac{10^{b}}{Bu_{rms}^{2/3}}\right)^{3/2} \quad (8)$$

The study uses the above equation to calculate the dissipation rate from ADV velocity measurements. This research uses for ***ε*** calculation *B* =1.5 (Pope, 2000).

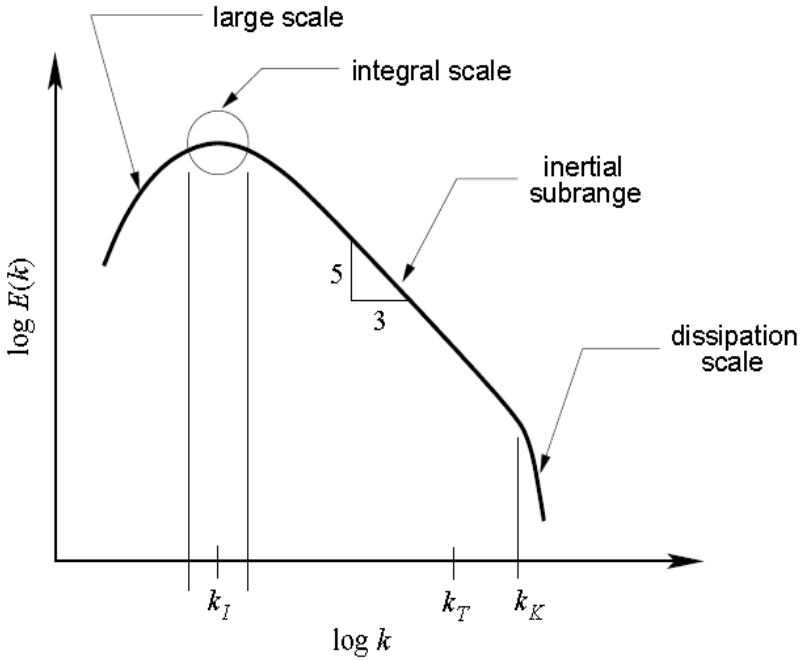

Figure 2. *Turbulent energy spectrum. The wavenumber k=2π/λ where λ is the wavelength of the signal (source: Bodyrev, 2007).*

2.4.2 Calculation of dissipation rate using ADCP's velocity profiles

Dissipation rate is calculated in this study using the 'structure function' technique proposed by Wiles et al. (2006). The method was derived from Kolomogrov theory and should be used only for the inertial subrange of the energy spectrum: $l_k << r << l_0$ (l_k is the scale of energy dissipation and l_0 is the vertical scale of the largest energy containing eddies). The method states that the second order structure function *(D(z,r))* can be described at any depth ***z*** using the fluctuating component of velocity ***u':***

$$D(z,r) = \overline{(u'(z) - u'(z+r))^2} \quad (9)$$

The above function is therefore the mean-square of the velocity fluctuation difference between any two points separated by a distance ***r***. This result, obtained by Wiles et al. (2006), assumes that the velocity difference is largely due to eddies of the length

scale equal to ***r***. It was argued (Taylor cascade theory) that the characteristic velocity scale is related to the dissipation rate and thus the structure function is:

$$D(z,r) = C_v^{\,2} \varepsilon^{2/3} r^{2/3} \quad (10)$$

where $C_v^{\,2}$ is a constant equal to 2.0-2.2 (Sauvageot,1992). It must be stated that the above result holds only when considering isotropic turbulence within its inertial sub-range. The detailed description of the method and its limitations can be found in Wiles et al. (2006). In order to calculate the dissipation rate from eq.10 a straight line is fitted to D(z, r) vs. along a beam distance:

$D(z, r)=N+Ar^{2/3}$

where ***N*** is an offset representing the uncertainly due to noise and $A = C_v^{\,2} \varepsilon^{2/3}$.

Rearranging the last equation the dissipation rate can be found from:

$$\varepsilon = \left(\frac{A}{C_v^{\,2}} \right)^{3/2} \quad (11)$$

In this study $C_v^{\,2}$=2.1 is used.

2.4.3 Reynolds Stress and TKE Production

It is possible to obtain the value of Reynolds stresses directly from Acoustic Doppler Velocimeter measurements. Firstly the Reynolds decomposition must be made in order to find the fluctuating part of the velocity: *u(t)=U+u'(t)* where U is the time average of the velocity and *u'* is its fluctuating component. The Reynolds stress could be calculated by multiplication and averaging of two fluctuating components: $\overline{u'w'}$ and $\overline{v'w'}$ (where the bar denotes a mean value). It must be stated that the covariance of the fluctuating parts of the velocity vector should be negative in the turbulent BBL. The turbulent eddies associated with events originating at the wall causes *w'* to be negative when *u'* (or *v'*) is positive. The product of the two (covariance) is thus negative. The stress can be obtained by multiplying the Reynolds tensor by density (*ρ*) of the fluid and minus one:

$$\tau_{xz} = -\rho\overline{u'w'} \text{ and } \tau_{yz} = -\rho\overline{v'w'} \quad (12)$$

Another approach to calculate Reynolds stresses was proposed by Lohrman (1990) for use with four an ADCP consisting of four beams. Details of the technique and the errors associated with it could be found in Stacey et al. (1999). The technique relies on the along-beam variances of the velocity measurements and therefore is called

the ‘variance method’. Opposite beams of the ADCP (see the next chapter for the device description) sample the flow at the locations that could be separated by several meters. Therefore, each beam can sample different turbulent eddies and this causes the correlation to be meaningless (Stacey et al. 1999). It is more convenient to use a ‘variance technique’, which relies only on the statistics (mean and variance) of the opposite beams:

$$-\overline{u'w'} = \frac{\overline{u'_3{}^2 - u'_4{}^2}}{2\sin 2\theta} \quad \text{(13) Stream Reynolds stress}$$

$$-\overline{v'w'} = \frac{\overline{u'_1{}^2 - u'_2{}^2}}{2\sin 2\theta} \quad \text{(14) Cross-stream Reynolds stress}$$

where u'^2_i (i=1,2,3,4 is the number of beam) are beam variances, θ is the angle between the vertical and the beams (20^0 for ADCP used in this research). The method requires the flow to be homogenous in the mean and variance of the velocity record, and stationary. The averaging period must be of sufficient length to provide a good sample of the largest eddies in the flow. In this study an average of 20 minutes is used as a compromise between stationarity and turbulence. The production of the turbulent energy can be calculated from the product of velocity shear and Reynolds stress:

$$P = -\tau_{xz}\frac{\partial \bar{u}}{\partial z} - \tau_{yz}\frac{\partial \bar{v}}{\partial z} = -\rho\left(\overline{u'w'}\frac{\partial \bar{u}}{\partial z} + \overline{v'w'}\frac{\partial \bar{v}}{\partial z}\right) \quad \text{(15)}$$

where *u* and *v* are stream and cross-stream components of velocity vector and the bar denotes time average values. Negative values of turbulent production (***P***) were found to be a result of the noise and thus are an indicator about the quality of data (Rippeth et al., 2003). The threshold value of P, when using a 1200kHz ADCP, was estimated to be ~7E-5 W/m^3 (~7E-8 W/kg) (Rippeth et al., 2003).

3.0 METHODOLOGY

3.1 Collection of data

The observations presented in this paper were collected during the night on 22/23 June 2006 from Plymouth Sound (Figure 3). Plymouth Sound is a part of the estuarine system that is the region of international importance owing to a variety of salinity and sedimentary conditions and marine habitats present here. Previous observations showed that the main currents in the area have north-south direction. The measurements took place when spring, flood tide occurred. The water depth at the site varied between ~ 9m at low water and ~12 m at high water. During the deployment the sea state was quiet with only little wave activity. The location was selected as having a flat bottom and being far from any topographic features. An underwater camera was used to check for any bottom irregularities that could cause disruption to the near-bed flow.

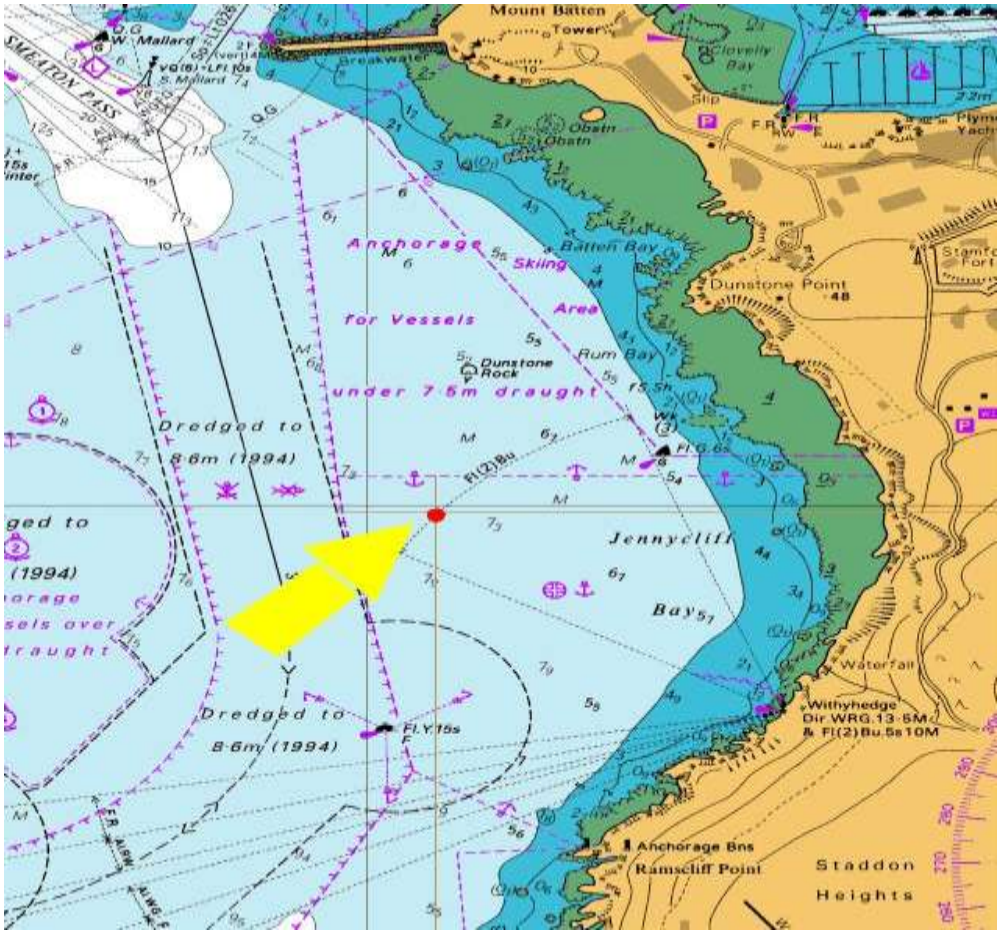

Figure 3. *The site of deployment pointed by the yellow arrow, the exact position shown in red- 50 20'59.6 N, 4 07'50.3 W (source: Admiralty Chart: Plymouth Sound and approaches, 2007).*

A frame, with an Acoustic Doppler Current Profiler (ADCP) 1200kHz (RDI Instruments) and two Acoustic Doppler Velocimeters (ADV), was lowered from the boat and placed at the sea bed. The equipment is shown in Fig 4. The Particle Tracking Velocimetry System (PTV), visible in Fig.4, was also attached to the frame, as part of a different project carried out at the same time. The orientation was changed to ensure that all the instruments were unaffected by the wake from the frame (Figure 5). An example of resulting changes in the orientation of the ADV is shown in Table 1. Additionally to the above instruments, currents in the whole water column were measured using a lower frequency (600kHz) ADCP attached to the boat. Salinity and temperature were profiled every 30 minutes and as a result 12 profiles were obtained. The time of each instrument operation is shown in Figure 5. The time difference in operation between the devices was recorded and used to create a time base for all instruments. The time of the ADV operation was chosen to be the reference time.

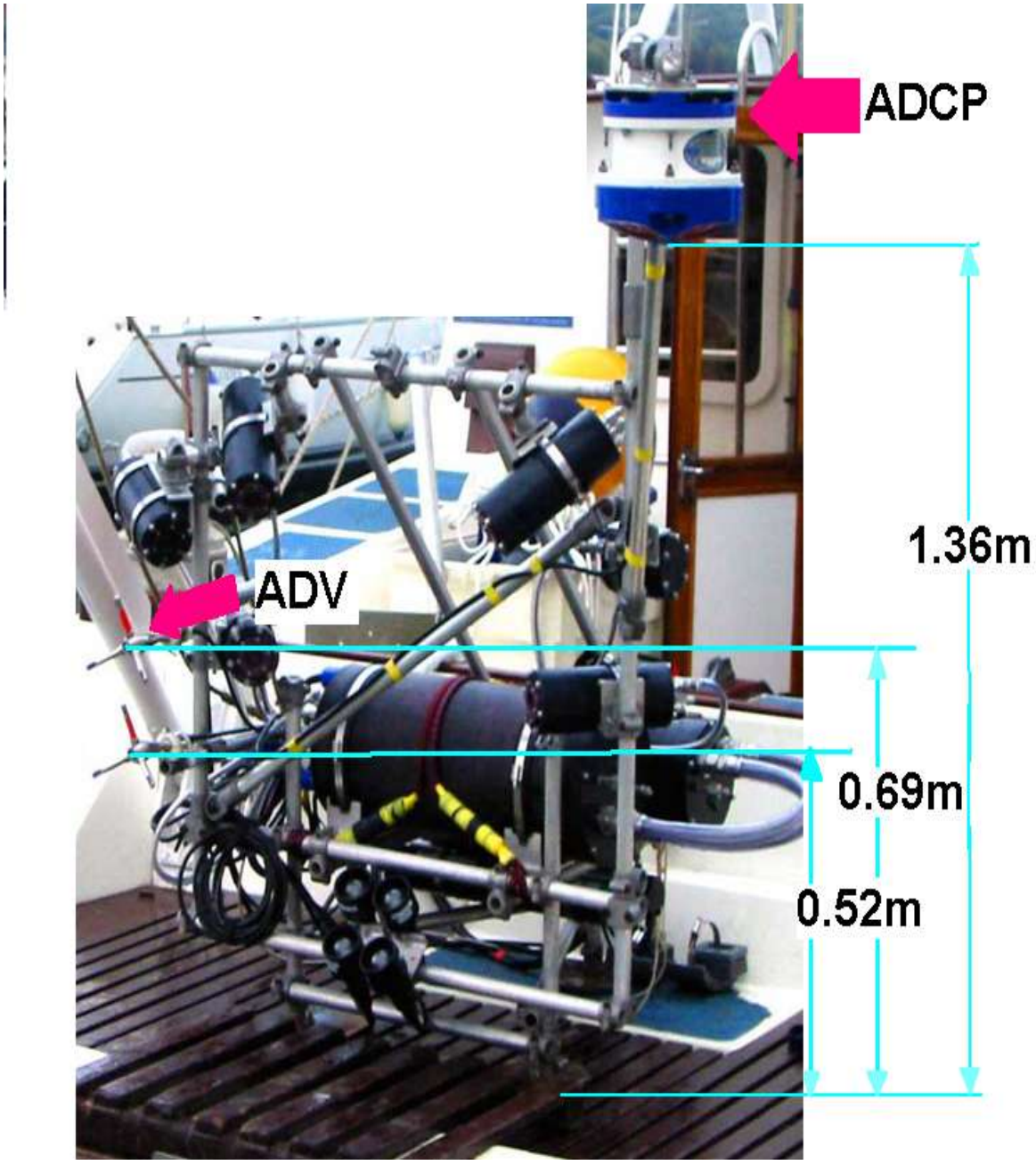

Figure 4*. The instrumentation used during the deployment. The height of the instruments is shown at the right side of the image. The instruments used for measurements are shown by red arrows. The rest of the equipment is the Particle Tracking Velocimetry system used simultaneously in a different study.*

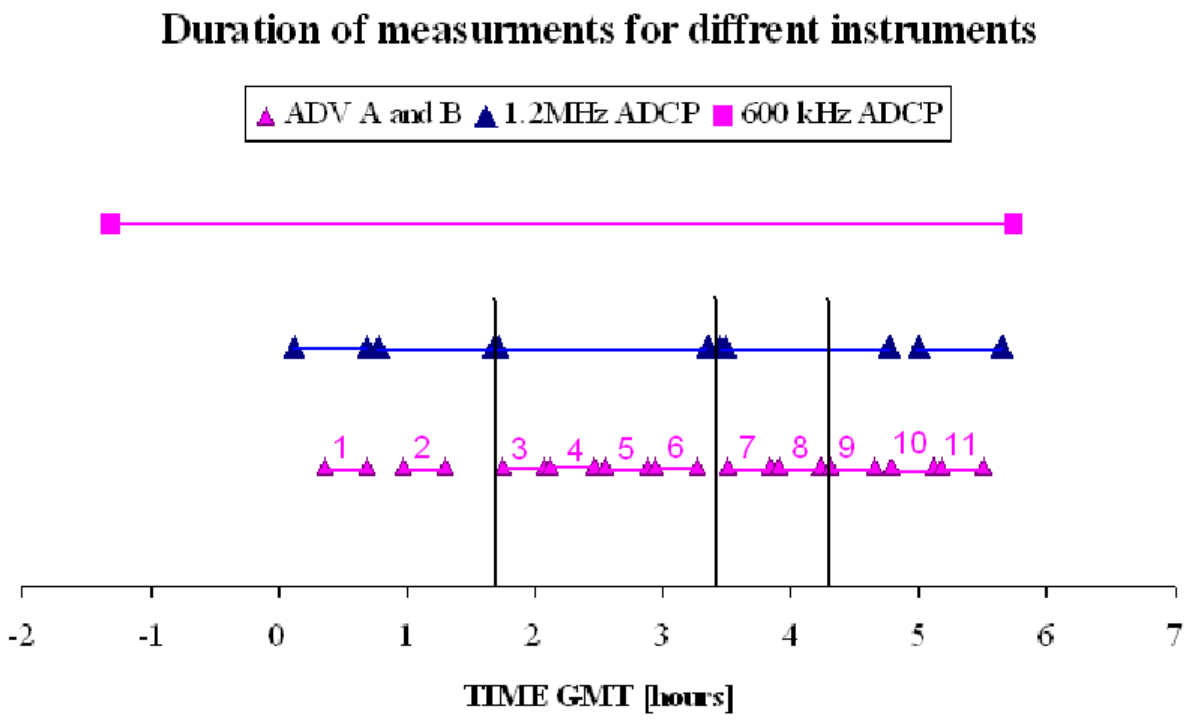

***Figure 5**. Measurement times. Notice a missing data in 1.2MHz ADCP recording during run 10 of ADVs. Black, vertical lines indicate the change in the instruments' orientation performed to align the sensors with the flow direction.*

run no.	heading	pitch	roll
1	345	-0.15	-1.63
2	345	-0.01	-1.73
3	8	2.95	-2.68
4	8	2.95	-2.73
5	8	2.99	-2.71
6	8	3.03	-2.8
7	50	1.22	-2.21
8	50	1.24	-2.26
9	87.5	-0.4	-2.28
10	87.5	-0.38	-2.35
11	87.5	-0.36	-2.39

***Table 1.** The orientation of ADV A during the deployment. Notice the change in the orientation after run 2, 6, 8.*

3.2 Instrumentation

3.2.1 Principles of Operation

Both types of acoustic devices used for the collection of velocity data (ADCP and ADV) operate using a principle of the Doppler shift. Their transducers transmit sound waves at fixed frequency, which bounce off the particulate matter suspended in the water. If the particles are moving toward acoustic receiver, sound waves are compressed which means they have a higher frequency. Therefore the device receives a bounded sound wave of different, shifted frequency. The shift in the frequency can be calculated from:

$$F_{doppler} = -F_{source}\frac{V}{C}$$

where: $F_{doppler}$ is the change of frequency (Doppler shift), F_{source} is the frequency of transmitted sound, V is the velocity of suspended particles and C is the speed of sound in the fluid. The above relationship is used to calculate three-dimensional velocity of the suspended particles. The ADCP uses multiple beams for this calculation (see section 3.2.3). The velocity of the flow is assumed to be equal to the velocity of scatters, which mostly move passively with the flow. However, the presence of fish or other sound scatterers, whose mean movement is not due to oceanic advection, will bias the velocity measurement (Plimpton et al., 1999). It was also argued that eddies smaller than the sensor volume are averaged because the effect of one side of the eddy is cancelled by that of the other side (Williams & Simpson, 2004).

3.2.2. Acoustic Doppler Velocimeter

An acoustic Doppler Velocimeter consists of a sound emitter, three sound receivers and a signal conditioning probe (Figure 6). The radial velocities are computed using the Doppler relation and converted to a local Cartesian coordinate system (V (x, y, z)) using the transformation matrix determined during a calibration by the manufacturer (McLelland et al., 2000). Signals of a higher frequency than the sampling frequency (f_s) of the instrument operation are filtered out thus the largest frequency resolved by the device is a half of the sampling frequency, the Nyquist frequency ($f_s/2$) (Garcia et al., 2000). The ADV averages N values of velocity producing the sampling frequency equal to the user-set frequency: $f_u=f_s/N$ (Garcia et al., 2000). The instrument was

proved to provide a good description of turbulence when certain conditions, related to instrument frequency and flow conditions, are satisfied: (Garcia et al., 2000).

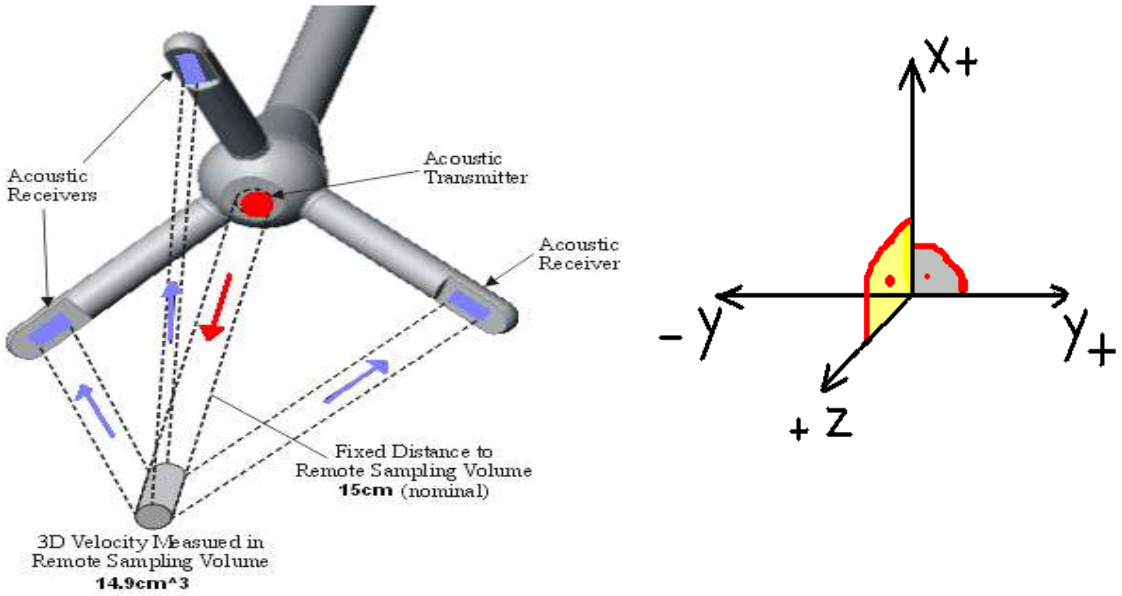

Figure 6. *The head of Acoustic Doppler Velocimeter and its orientation as used in this study. Principle of operation is shown on the left. The sound transmitter and transmitted signal is marked in red whereas returned signal and receivers are marked in blue. The orientation of the system in the Cartesian coordinate system is shown on the right. The x axis is the vertical and y and z are horizontal axes. (source: Johanes Keppler University, 2007)*

During the deployment, the two ADVs, which were attached to the frame at 69cm (ADV A) and 52cm (ADV B) above the bottom, measured three components of the velocity vector in x, y and z direction at the sampling frequency of 25Hz (Figure 6). Furthermore, noise amplitude and correlation were recorded. The compass located in the main body of each ADV recorded the sensor's orientation: pitch, roll and heading. The velocity was measured in the sampling volume equal to 14.9 mm^3 located 15cm from the transducer (Figure 6). Twelve, 20 min long runs were recorded by each ADV (Figure 5). The third run was rerun again because the frame was moving up and down above the bottom during that period.

3.2.3 Acoustic Doppler Current Profiler

An ADCP measures the velocity by assuming that the velocity is homogenous in the respective depth cells. Each beam of an ADCP measures the velocity in one direction, therefore to measure three-dimensional velocity three beams are needed. Figure 7 shows how four-beam ADCP measures the velocity vector in the Earth coordinates (East, North and Vertical). As one can see in Figure 7, vertical velocity is estimated using all four beams. The difference between the two estimates of vertical velocity is called the error velocity. It provides useful information, whether the assumption of horizontal homogeneity is reasonable. Firstly, an ADCP measures velocity in the beam direction and then transforms it to Earth coordinates. During this operation the ADCP corrects for the angle of the beams as well as any movement of the sensor. Depth cell mapping is used in order to compute the velocity from the same depth.

The echo intensity near the boundary (sea surface and bed) is much stronger than the echo from scatters present in the water, which could overwhelm the side lobe suppression of the transducer. For the 20^0 transducer, 6 % of the data adjacent to the sea bed is rejected which is called the bottom blanking distance (Gordon, 1996). Furthermore, a flow pattern close to the transducer is affected by the presence of the device. Therefore the velocity measurements are biased towards zero near the instrument. To reject the biased values one must choose the size of top blanking distance, in the device settings, which tell the instrument how much of the top profile should be rejected. The size of the top blanking distance is the function of flow velocity, instrument frequency and mode of operation. The lower the flow velocity, the smaller the size of the blanking distance.

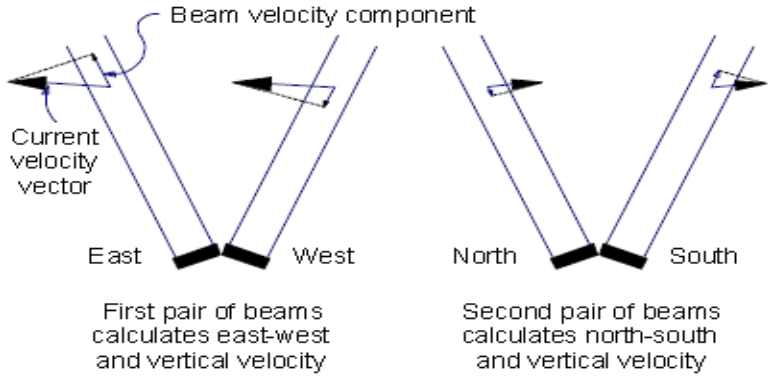

***Figure 7**. The relationship of Earth and beam velocity (Source: Gordon,1996).*

The ADCP divides the water column into a number of uniform depth cells (bins). The average velocity is measured in each bin and the resultant value is obtained in the middle of each bin. The regular spacing makes the data collected much easier to process and reduces the effect of spatial aliasing. However, smoothing the velocity in the vertical causes loss of velocities that have their vertical variation smaller than the depth cell. On the other hand, the averaging reduces measurement uncertainty (Gordon, 1996). It must be noted that the adjacent segments overlap each other by 15% and the averaging is most sensitive to currents at the centre of each bin (Gordon, 1996). This type of velocity measurement has two types of error associated with it: random error and bias. The averaging reduces random error but not a bias. To remove the bias the device must be calibrated and the random error can be estimated by computing the standard deviation of the error velocity.

Two four-beams, downward-looking ADCPs collected three velocity components (East, North and Vertical) in the 'Earth' coordinates simultaneously with the ADVs, but the data recorded was longer in duration (See Figure 5). They provided the record of three dimensional velocity vector, the echo amplitude and correlations between the four beams (Table 2). The movement of each instrument was recorded by the compass and pressure sensor. In addition, the 600kHz ADCP attached to the boat measured the range to the bed during the time of deployment. The high frequency ADCP profiled the currents in mode 11 and the lower frequency ADCP in a default mode 1. Mode 11 is a 'Pulse to Pulse coherent' mode. It provides a high resolution measurement and 10 to 100 times higher precision than mode 1 (RD Instruments, 2002). It allows the bin size to be as small as 1cm but it may not work if the depth (m) times velocity (m/s) product is greater than one (RD Instruments, 2002). Therefore mode 11 is recommended for the boundary layer studies or shallow water profiling in rivers and estuaries (RD Instruments, 2002). The main differences between the devices used in this study are shown in Table 2.

	600 kHz ADCP	1.2MHz ADCP	ADV
Sampling frequency	1.11 Hz	1.58 Hz	25 Hz
Bin size/sampling volume	0.5 m	0.02 m	14.9 cm^3
Mode	1	11	N/A
Top blanking distance	1.5 m	0.2 m	N/A (15 cm from transducer head)
Main Measurements	3D velocity Velocity direction and magnitude Echo amplitude Pitch, Roll, Heading Range to the bottom Pressure Temperature	3D velocity Velocity direction and magnitude Echo amplitude Pitch, Roll, Heading ---------- Pressure Temperature	3D velocity echo intensity pressure pitch, roll, heading
Record time	7 hours measured continuously	11 records each more than 20 min long	11 records each 20 min long

Table 2. *Summary of the instruments settings and the data collected by them.*

3.3 Methods used to process the raw data

3.3.1. ADV data

The ADV informs about data quality by outputting values of checksum and velocity correlation. The data that has a checksum equal to 1 indicates low quality and thus was removed. Also velocities with correlation lower than 70% were not used in further analysis. It was found that only a small percent of data qualified for elimination. Furthermore some of the velocity records had many very high, single values (about 1m/s), which could be caused by marine organisms. The velocities greater than three standard deviations were removed together with the two adjacent values. The data was then linearly interpolated across these places. The spikiest records, where up to 28 spikes were removed from the x component of velocity, were collected during the end of deployment. The velocities were transformed from Cartesian (x, y, z) to stream (u, v, w) coordinates by rotating about z and y axes using a transformation matrix (See Figure 6 for instrument geometry). The angle of the translation for all transformations was about 6^0 in y direction and about 2^0 in z. The rotation assumed that the mean vertical velocity is zero and thus calculates stream and cross-stream velocities from x,y,z velocities. The Reynolds stress was calculated from u,v,w as described in section 2.4.3. The TKE production was calculated by averaging the mean u'w' at two ADVs' elevations and multiplying by the velocity gradient (du/dz).

Time series of the resultant velocities were plotted and their cumulative means were calculated to check if the cumulative mean converged during the duration of each record. The procedure gave information about the statistics of each dataset; was the record long enough to resolve turbulence from it? The next step in the processing was to calculate a dissipation rate for each component of velocity vector. The trend from each record was removed and one sided power frequency spectrum was obtained using a Welch method ("pwelch" function in Matlab). A Hanning window (length: 1024 with 50% overlap) was used before performing Fast Fourier Transform (FFT) because it gradually reduces the amplitude of the ideal-impulse response towards zero at the edges of the window, therefore reduces ringing effects caused by the window. The dissipation rate was calculated using the method described in section 2.4.1: a straight line (-5/3 slope) was fitted to the power frequency spectrum

of each velocity component plotted in the log-log scale. The results of energy dissipation rate where scaled as u'=3/4 w' and $\varepsilon_{u'} = ¾\ \varepsilon_{w'}$.

3.3.2. ADCP data

The velocities measured by 1200kHz ADCP in the beam coordinates were used for the calculation of Reynolds stresses and the rate of turbulence energy dissipation as described in sections 2.4.3 & 2.4.2. Firstly, the low quality data (indicated as -32768mm/s) was removed from the record and replaced by linear interpolation between the nearest two good values. Then the velocity measured by each beam was divided to its mean value (*U*) and fluctuating part (*u'*). In order to calculate dissipation rate using Wiles' et al. (2006) method the 'centred difference' technique was used (from 1 to10 data points) to obtain velocity difference for each depth cell (See section 2.4.3 for the method description). The resultant differences were squared and averaged over 20 minutes period corresponding to the operational time of the ADV. The production of turbulence was calculated by multiplying mean *u'w'* by velocity magnitude shear for each bin.

The same procedure of removing low quality data was used to process the measurements from both ADCPs transformed to Earth coordinates. The sea bed was used as a vertical reference frame and therefore the height of each measurement was converted to the height above the bed. The mean value of bottom range collected by each beam of 600kHz ADCP was used for this transformation.

3.3.3. Conductivity and temperature data

Temperature and salinity profiles collected by CTD probe were used to calculate water density. The formula used for this calculation was taken from Pond& Pickard (2005). Obtained density was averaged in 0.5-meter depth cells corresponding to ADCP bins. The buoyancy frequency and Richardson number ware then calculated using the equation 1 from section 2.1. That was estimated using east and north components of velocity vector collected by the low frequency ADCP. In order to find the gradients of velocity the 'centred difference' technique was used with vertical length (Δz) equal to 0.5m.

4. RESULTS and DISCUSSION

4.1 Degree of Stratification

Contour plots of temperature, salinity and density are shown in Figures 8-10. It can be seen that at the low water (LW) salinity increased with depth from 34.9 at the surface layer to 35.4 near the bottom. At the start of the flood, the water became less saline at the top layer of the water column (34.6) and the depression in the height of the most saline water can be observed. During further increase in the sea surface elevation, the volume of most saline layer near the bottom (35.4) raised proportionally to sea surface elevation. Furthermore, it can be noticed that the salinity in the first two meters above bottom was constant, about 35.4, during the time of deployment. Vertical structure of temperature for the same duration is shown in Figure 9. The visual inspection shows that temperature changed very little at LW and at the start of the flood. Its value ranged from about 14.6^0C near the bottom to 14.7^0C just below the sea surface. After two hours, the water located near the bed became colder (13.8^0C) which caused the warmer water to rise because it was lighter. The intrusion of cold water was progressing, increasing its volume in the water column. In a consequence a two layer structure was formed with cold water below the warm. The maximum difference between the temperatures was found to be about 1^0 C.

It can be seen in Figure 10 that the resultant density was the product of salinity and temperature. Because the temperature at the start of deployment was almost constant, density was mostly affected by salinity during that time and both showed similar profiles. However, temperature varied during a later time (2h-5.5h) which caused density to be a product of the two. As a result, denser water (1026.5 kg/m^3), located near the bottom, increased its volume in the water column proportionally to the increase in sea surface elevation. At the same time the less dense layer (1025.7 kg/m^3) was situated in the top 4 m of the water column. The maximum gradient of density was found to be about 1kg/m^3. However, it can be observed that density was almost constant in the 2m layer next to the bottom during the whole flood.

The water column stability was parameterized in terms of gradient Richardson number which was calculated with 0.5m resolution. The Richardson number (Figure 11) indicated that there was enough kinetic energy in the flow to mix the water

column. Therefore it can be argued that density stratification was weak and the flow was turbulent. Generally, Richardson number was found to be positive (from definition) and less than 0.25, for most of the time, indicating that shear instabilities gave rise to turbulent mixing. This caused the water column to become well mixed during the flood. However, some values greater than one was found at 5 m above the bottom, mostly at the slack water. This means that the density gradient may stabilize the instabilities caused by the shear during that time. The results confirm Simpson's (1995) Strain Induced Periodic Stratification (SIPS) theory which says that the water column during the flood in the regions of fresh water influence should be completely mixed as a result of oceanic water flowing over less dense estuarine water.

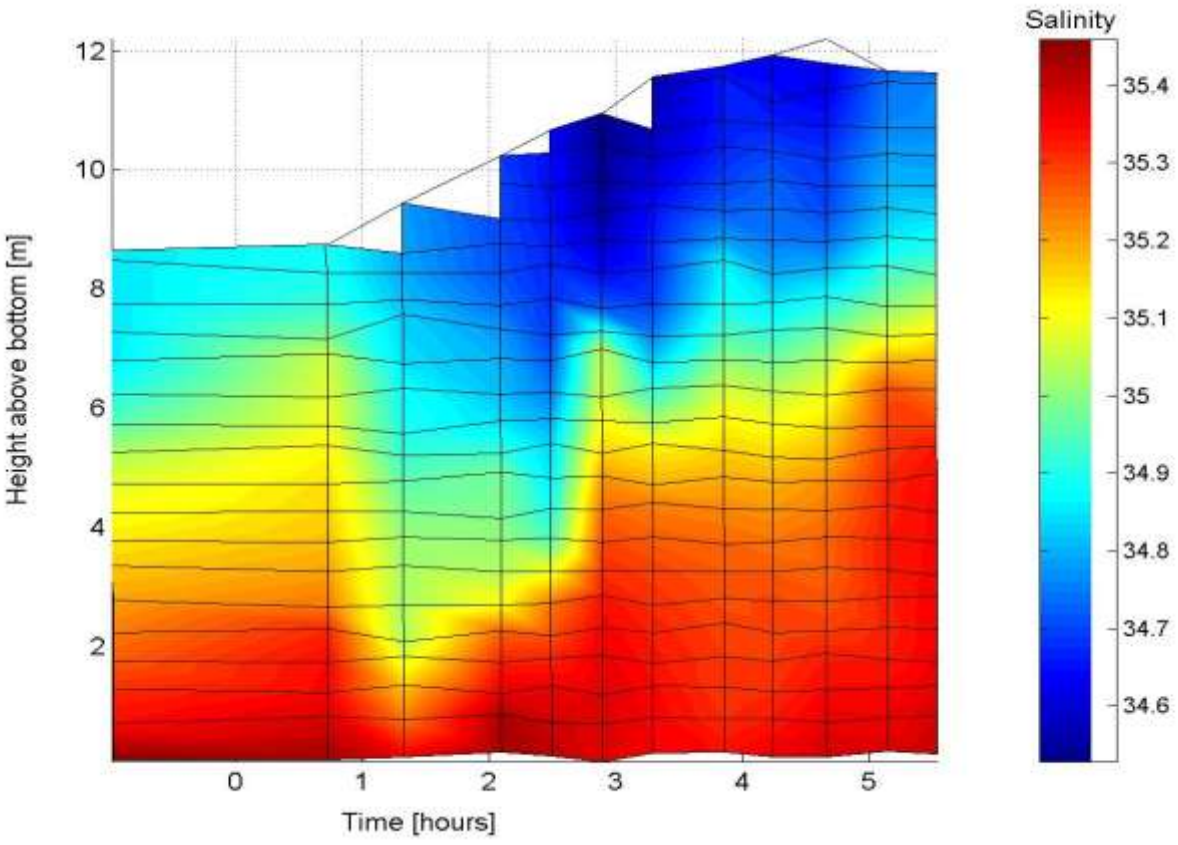

***Figure 8**. Changes in salinity during the deployment. The crossing of the lines indicates the real data points. Time equal to zero corresponds to 22pm of ADV time.*

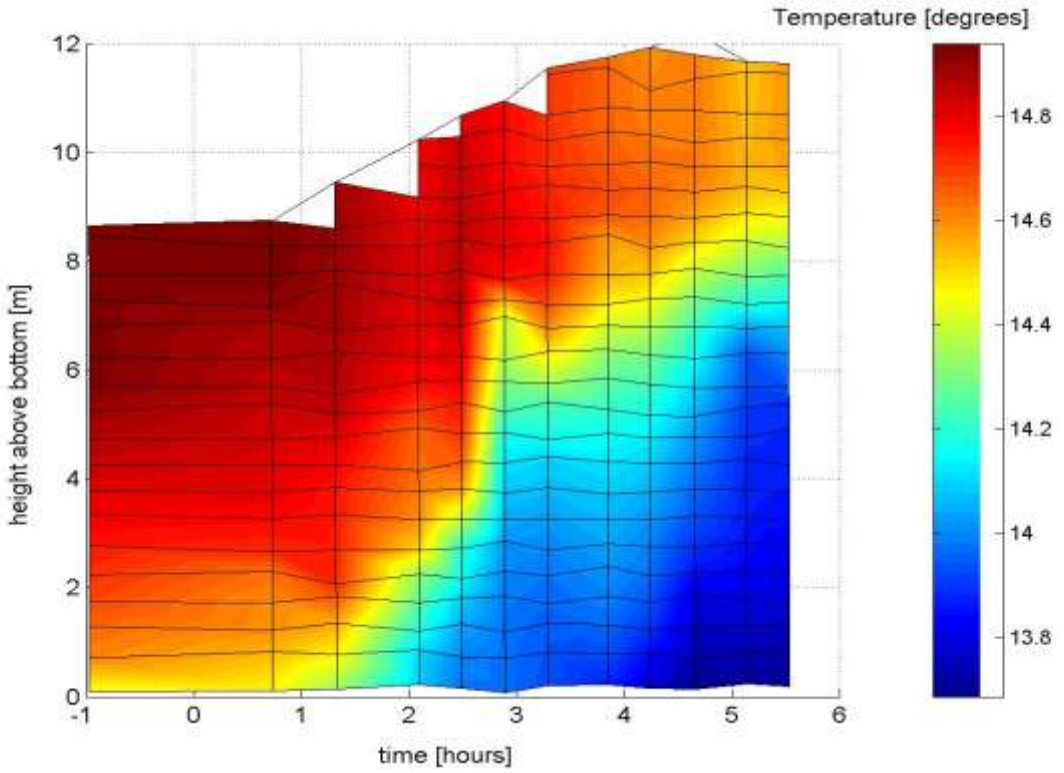

***Figure 9**. Changes in temperature during the deployment. The crossing of the lines indicates the real data points. Time equal to zero corresponds to 22pm of ADV time.*

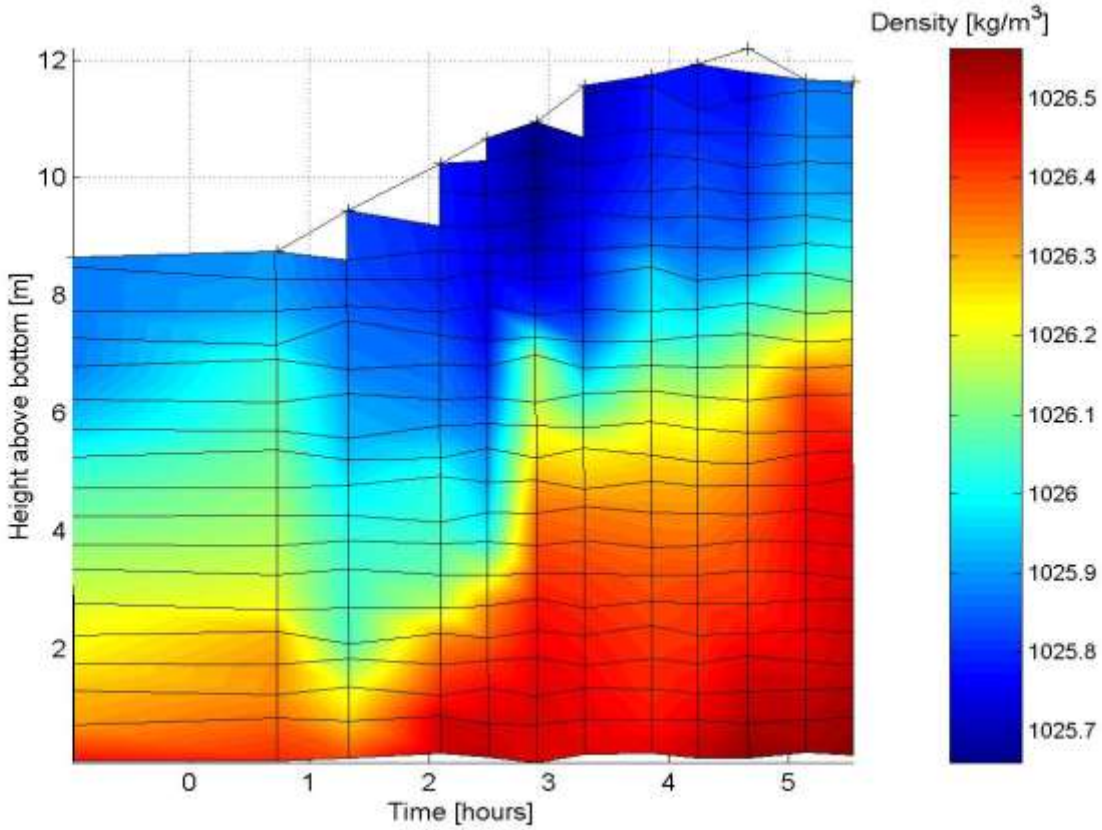

***Figure 10**. Changes in density during the deployment. The crossing of the lines indicates the real data points. Time equal to zero corresponds to 22pm of ADV time.*

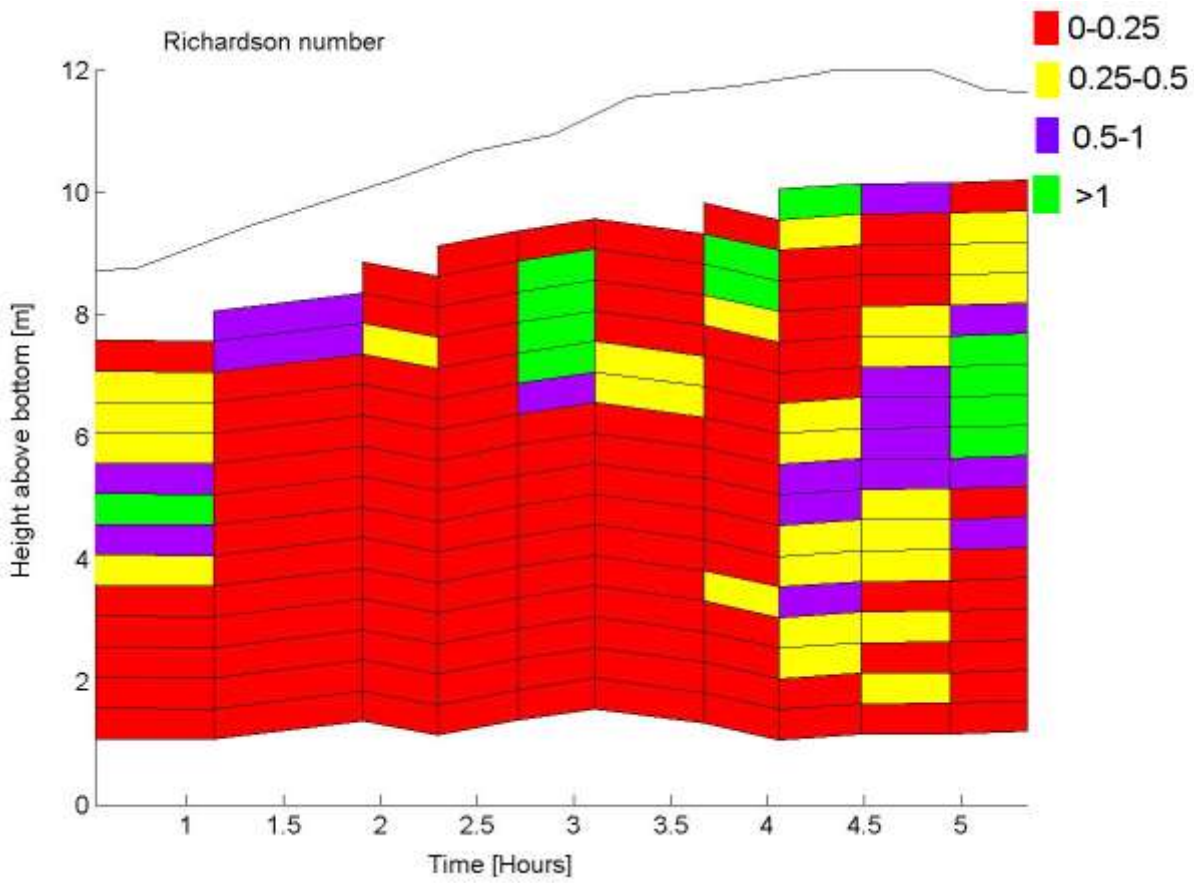

Figure 11. *Time series of Richardson number at different depths. The crossing of the lines indicates the real data points. Time equal to zero corresponds to 22pm of ADV time. Green squares indicate Ri>1.*

4.2. Flow Structure

Figures 12-15 show velocity profiles collected by two ADCPs, which measured velocities in the whole water column (600kHz ADCP) and in the top 1m above the bottom (1.2MHz ADCP). Because of the 600KHz ADCP's bottom blanking distance, which was found to be about 6% of the profiling range, the top ADCP did not measure the velocities below 1.5 m above the bottom. Therefore the measurements performed by the two ADCPs did not overlap each other. However, it can be seen in figures 12-15 that the measurements collected by the devices show the same magnitudes and directions and are in good agreement with each other.

The flow was found to be predominantly a result of semidiurnal tide which consisted of about 6 hours long, slow, flood tide with velocities up to 0.22m/s (Figure 12). The strongest velocities were found near the centre of the water column during the first three hours. After the velocities reached the maximum (~2h), the flow decelerated and became almost equal to zero. As a result, velocity magnitude did not vary much throughout the whole water column in the last two hours (0.02m/s-0.08m/s). During the beginning of the flood phase of a tide, it was observed that a direction of the flow was different at different depths (Figure 13). During the first hour the direction of the top 6 m was 220^0 whereas currents situated below 4m above the bottom flowed at 60^0. It was found that a lot of shear was produced during the first three hours of deployment. After that period of time the direction did not vary so much and changed from 160^0 near sea bed to 140^0 at the middle and top depths.

When considering the ADCP measurements, the mean direction and magnitude of the velocity is a product of two horizontal components of velocity vector: east and north (assuming mean vertical velocity to be equal zero). The horizontal components of velocity vector are shown in figures 14 and 15. It can be seen that both components reached their maxima in almost the same time (~2h) and at similar depths (~3m). The greatest values of north and east velocities were found to be 0.16 m/s and 0.13m/s respectively. However, after about three hours the north component became equal to almost zero, whereas the east reached 0.02 m/s near the bottom and 0.06 m/s above the centre of the water column.

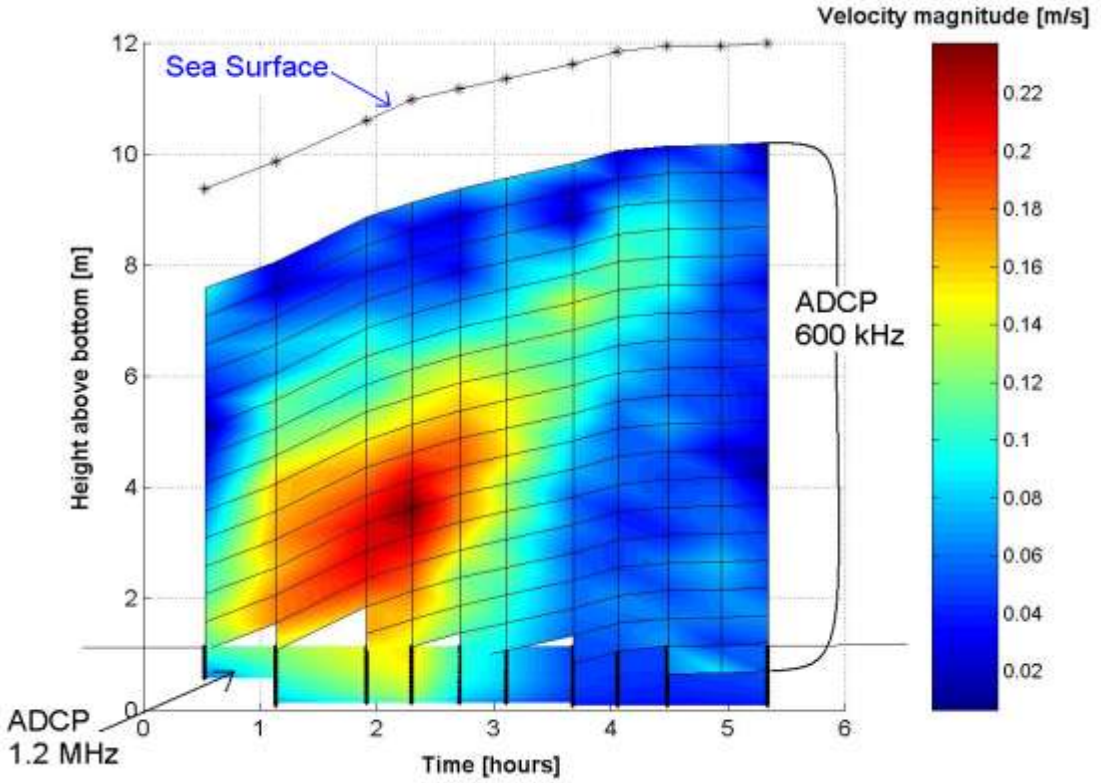

***Figure 12**. Profiles of magnitude of velocity vector during deployment. Sea surface elevation show in blue, top of the profile indicates velocities collected by 600kHz ADCP whereas the bottom part data collected by 1.2 MHz ADCP. Time equal to zero corresponds to 22pm of ADV time.*

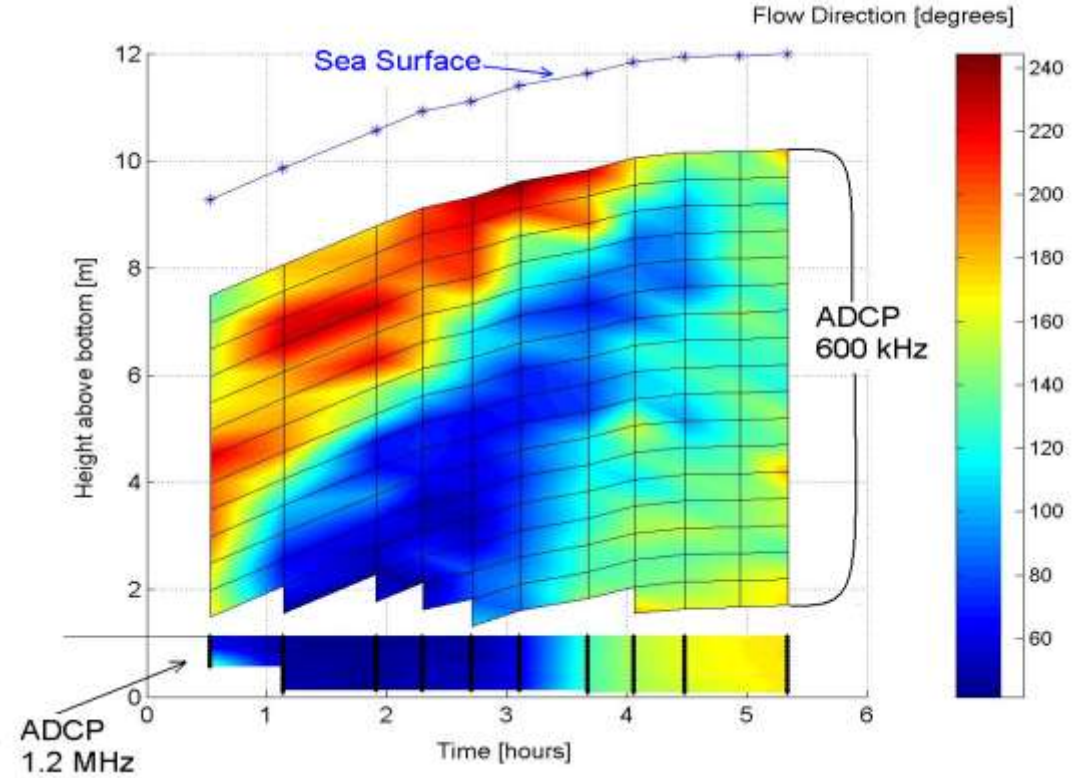

***Figure 13**. Flow direction during deployment. Sea surface elevation show in blue, top of the profile indicates velocities collected by 600kHz ADCP whereas the bottom part the measurements collected by 1.2 MHz ADCP. Time equal zero corresponds to 22pm of ADV time.*

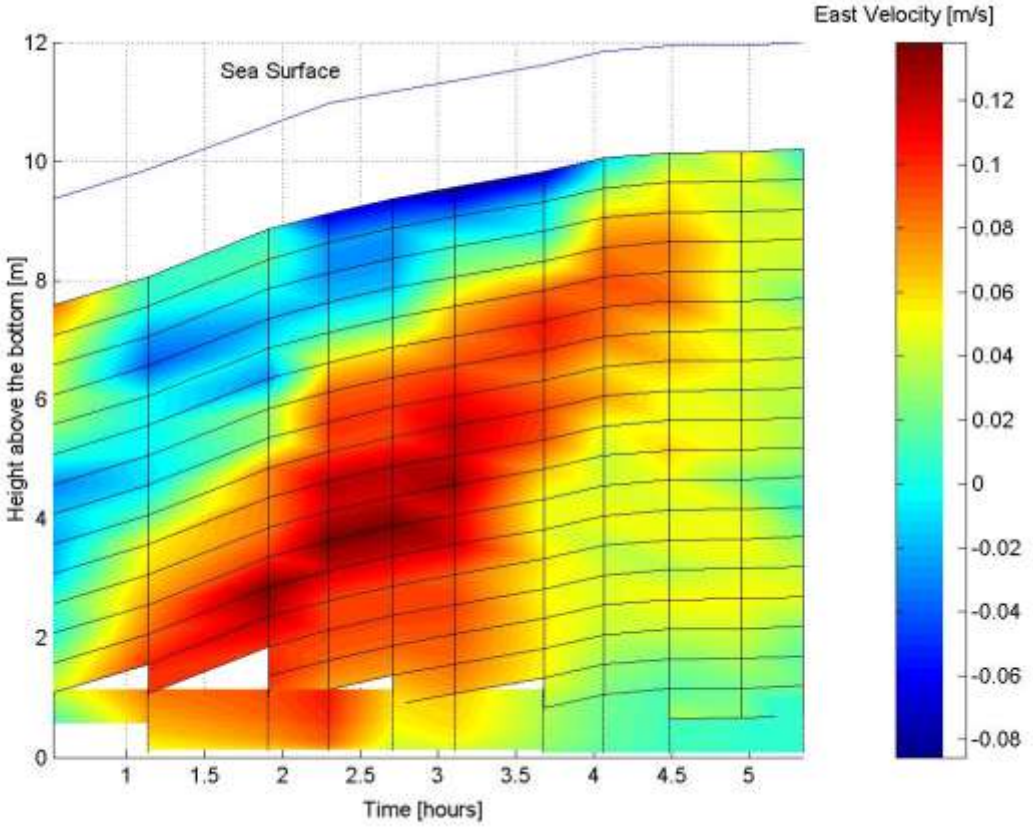

Figure 14. *Profiles of east component of velocity vector. The crossing of the lines indicates the real data points. Time equal to zero corresponds to 22pm of ADV time.*

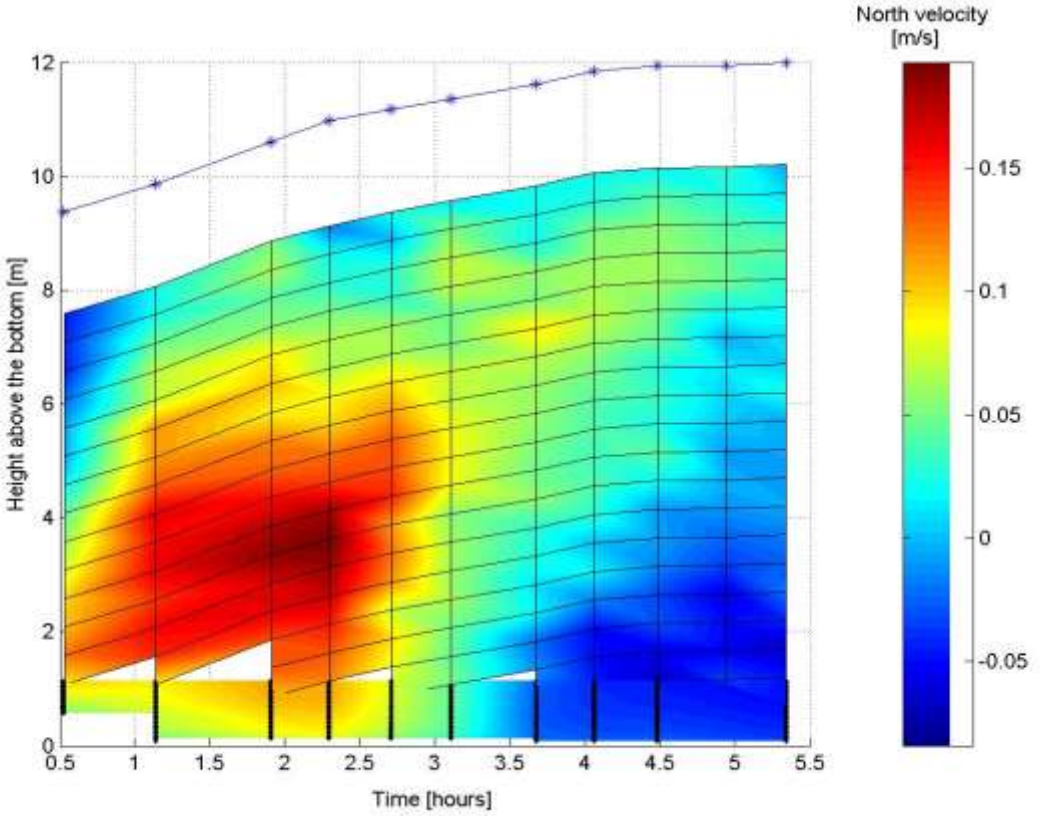

Figure 15. *Profiles of north component of velocity vector. The crossing of the lines indicates the real data points. Time equal to zero corresponds to 22pm of ADV time.*

Two ADVs provided information about the stream, cross-stream and vertical velocities (*u(t),v(t),w(t)*) at two different elevations (See Figure 4) . The magnitude of the velocity vector measured by both ADVs was consistent with the 1.2MHz ADCP measurements. As a result of the rotation, the vertical and cross stream components of velocity had a mean value equal to zero, whereas the stream component increased in the first two hours and reached the maximum of about 0.15m/s just after two hours of deployment (Figure 16). After peaking, the velocity decreased and reached 0.04 m/s after 3.5 hours, remaining at this level to the end of deployment. Figure 16 shows that two ADVs situated at different depths are in good agreement with each other and show the same trends in the mean *u(t).* The root-mean-square ($\sqrt{\overline{u_i'^2}}$ = $u'_{i\,rms}$) of fluctuating velocities (*u',v',w'*) was found to be almost the same for both instruments, considering stream and cross stream directions (Figure 17). However, greater difference between the instruments was observed for *w'*. Generally, u'_{rms} was found to be the largest (2-3 mm/s) and v'_{rms} and w'_{rms} had similar magnitude (1-1.5mm/s) in the first 3 hours of the deployment. However, after this time u'_{rms} became lower than the other two components (about 1mm/s) which suggests turbulence anisotropy during that time.

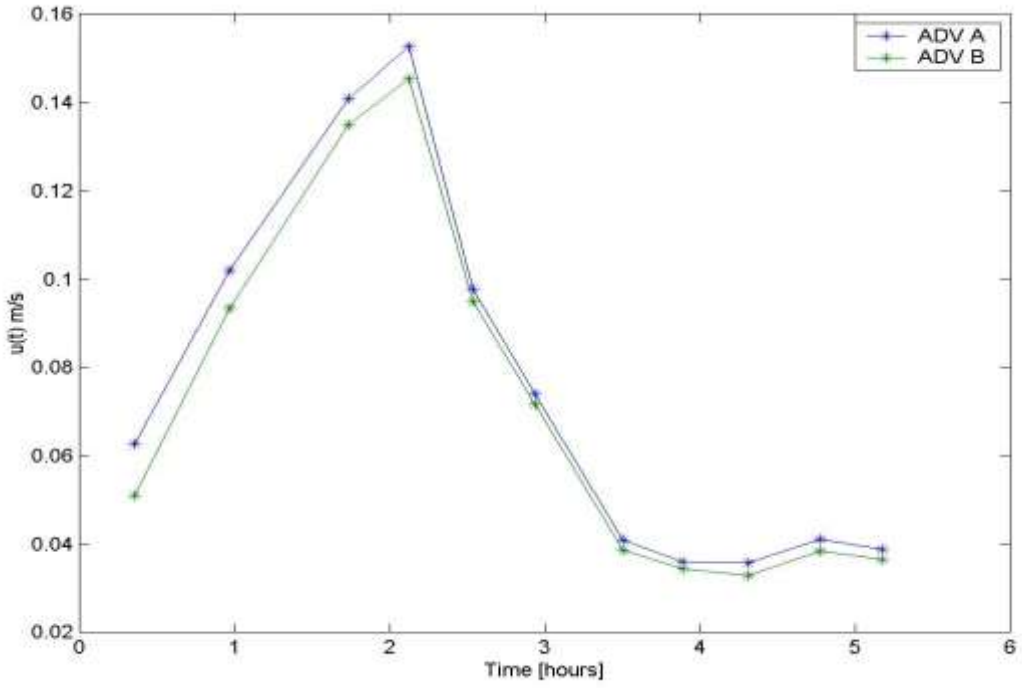

Figure 16*. Mean stream velocity (u(t)) changes during the flood tide at two elevations: ADV A (69cm above bottom) and ADV B (52cm above bottom). The cross-stream and vertical components of velocity have a mean value equal to zero.*

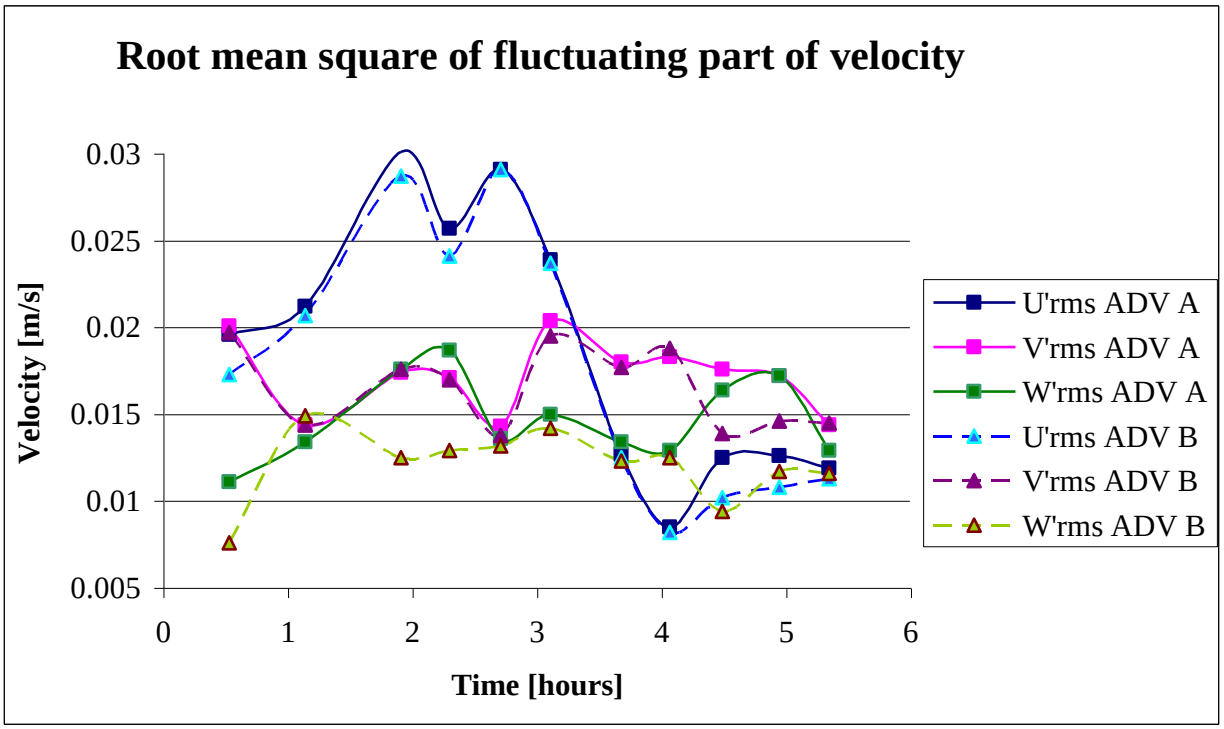

***Figure 17**. Root-mean-squared fluctuating velocities. Triangles indicates data points from ADV B and squares from ADV A.*

Examples of cumulative means are show in Figures 18 and 19. The convergence of the cumulative mean indicates that the averaging period has a sufficient length to provide a good sample of the largest turbulent eddies. However, it was found that during the first run the cumulative mean of cross-stream velocity did not converge. This could be a result of non-stationary flow during that time. In order to further process the data, the record was divided into 3 parts describing an acceleration and a deceleration in the flow. Then the trend was removed from each part of the record. All later records showed convergence in the cumulative mean. An example of a record with the convergence for *u(t), v(t), w(t)* is shown in Figure 19.

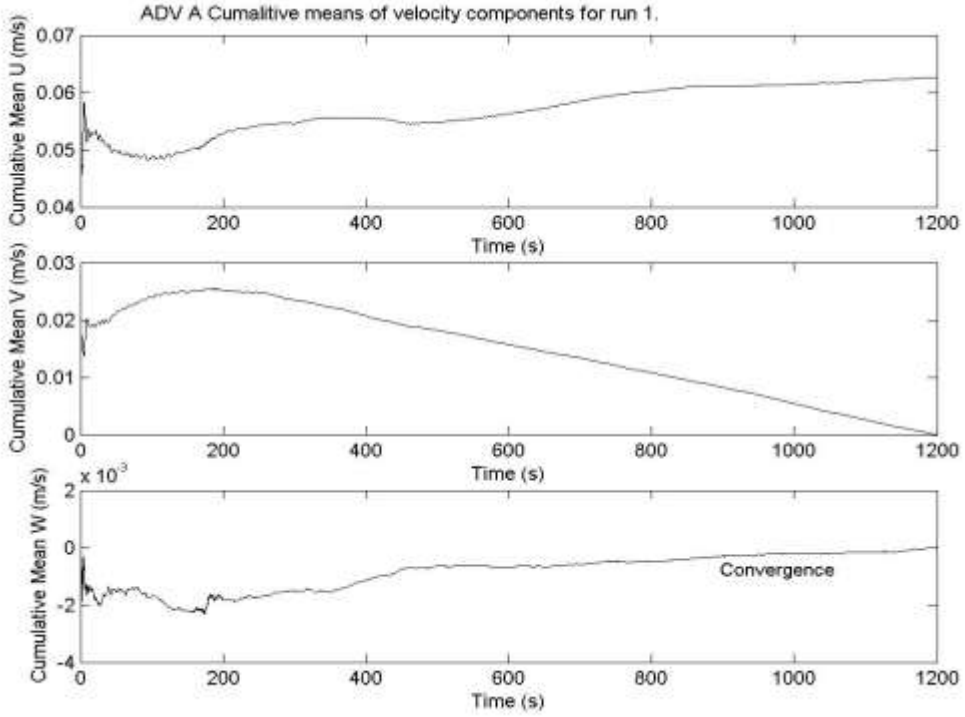

***Figure 18**. Cumulative means of velocity components during run 1. Notice that the cross stream component do not converge during 20 min period.*

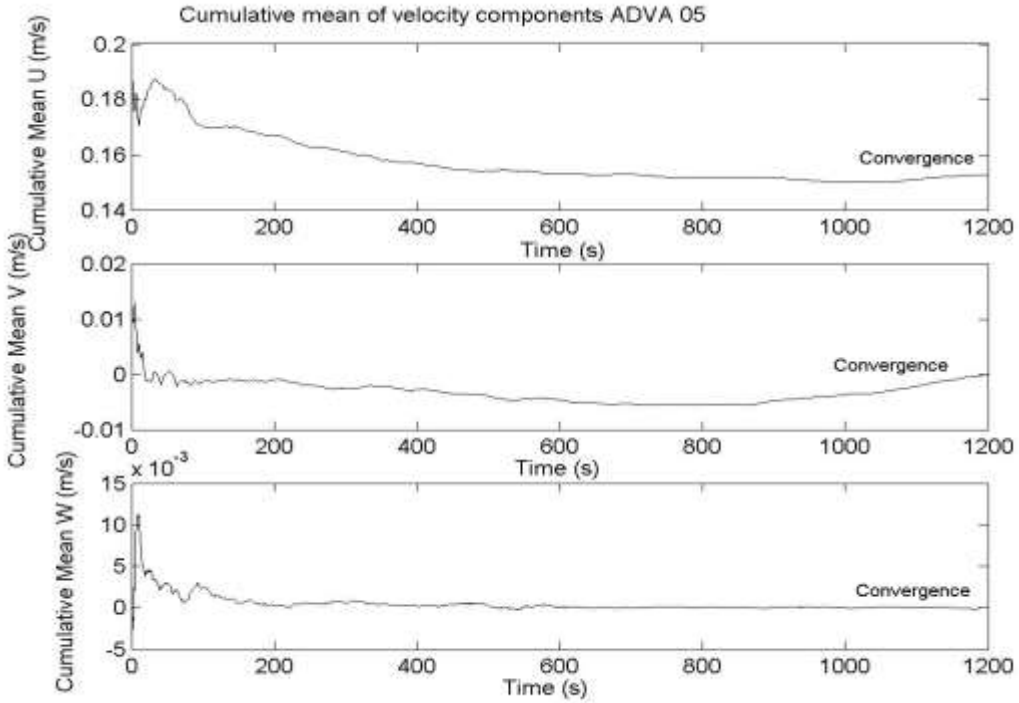

***Figure 19**. Cumulative means of velocity components showing convergence during 20 minutes period.*

During the deployment only small waves were observed. Frequency of waves was found by applying spectral analysis to the pressure record provided by the ADV and the 1.2MHz ADCP. Both instruments provided similar results, a peak wave period was found to be about 10s and did not change during the flood tide (Figure 20). Values of wave number calculated for this frequency suggest that intermediate water waves occurred during the deployment. The waves could bias turbulent characteristics. Therefore their effect will be discussed when considering the limitations of various techniques used in this study for calculation of TKE dissipation and production (Reynolds stress).

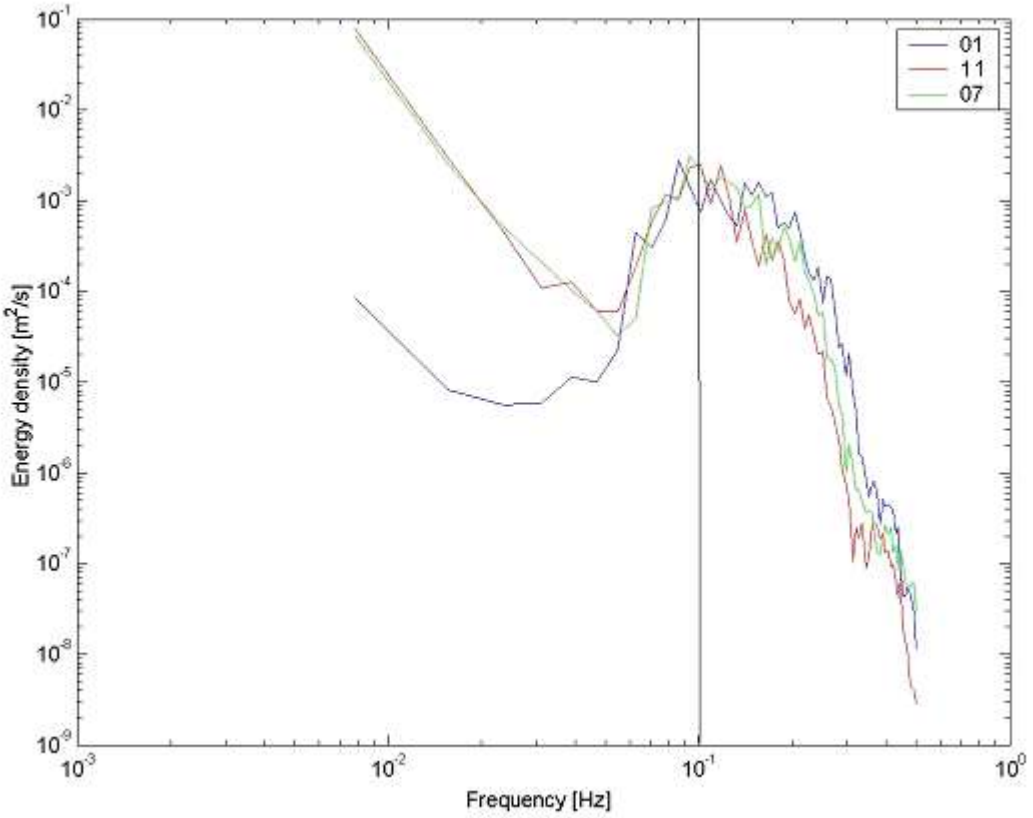

***Figure 20**. Log-log energy density spectra of pressure recorded by ADV A. The results show how the energy of wave changes in time: blue spectrum indicates the start of deployment, green the middle, and red the last measurement.*

4.3 Bottom boundary layer

The mean velocities in the first meter above bottom were obtained form the 1.2MHz ADCP. Figure 21 shows mean velocity magnitude profiles during the deployment. It can be seen that the velocity increased with height above the bed proportionally to the logarithm of the elevation. Therefore, the results agree with a theory, which says that the part of the profile of velocity in the BBL should have a logarithmic part (See section 2.2). During the first run, the high frequency ADCP range was limited (1.14m-0.66m) due to wrong instrument's settings. As a result, shear velocity and other parameters were not calculated for this run. The results were obtained by using the method described in detail in section 2.2 and are shown in Figure 21. The regression coefficient (R^2) greater than 90% (Table 3) indicates that the data fits into logarithmic law well. The coefficient was used as the indicator which part of the profile describes the log layer. The value of $R^2 > 90\%$ was used as a threshold value. It was found that almost all profiles had a logarithmic shape below 1.14m. Only during run 7 (3.67hours) the log layer ranged only up to 92cm above the bottom. Furthermore, it was found that the velocities measured by the 600kHz ADCP did not have a logarithmic part. This could be explained by two arguments: The log-layer range must be less than the range of the boat mounted ADCP (~up to 1.5m above sea bed) and greater than 1.14m above bottom (the first bin of 1.2MHz ADCP); or the 600kHz ADCP provided measurements of no sufficient accuracy to resolve the log layer in the BBL using the same method.

run no. ADCP 1.2MHz	**Regression coefficient [%]**	**equation y=ax+b**
1	98.6	y=0.0766+0.0991
2	98.5	y=0.0231x+0.1187
3	98.4	y=0.0216x+0.145
4	97.18	y=0.0187x+0.155
5	95.9	y=0.0128x+0.1021
6	91.1	y=0.0097x+0.0839
7	90.5	y=0.0046x+0.0505
8	97.2	y=0.0051+0.0485
9	96.9	y=0.0064x+0.0482
10	98.5	y=0.0084x+0.0556

Table 3. *The equation describing velocity profile in the log-layer obtained using regression analysis to fit the straight line into velocity [m/s] versus natural logarithm of elevation [m]. Regression coefficient shows how well the data fits into the model.*

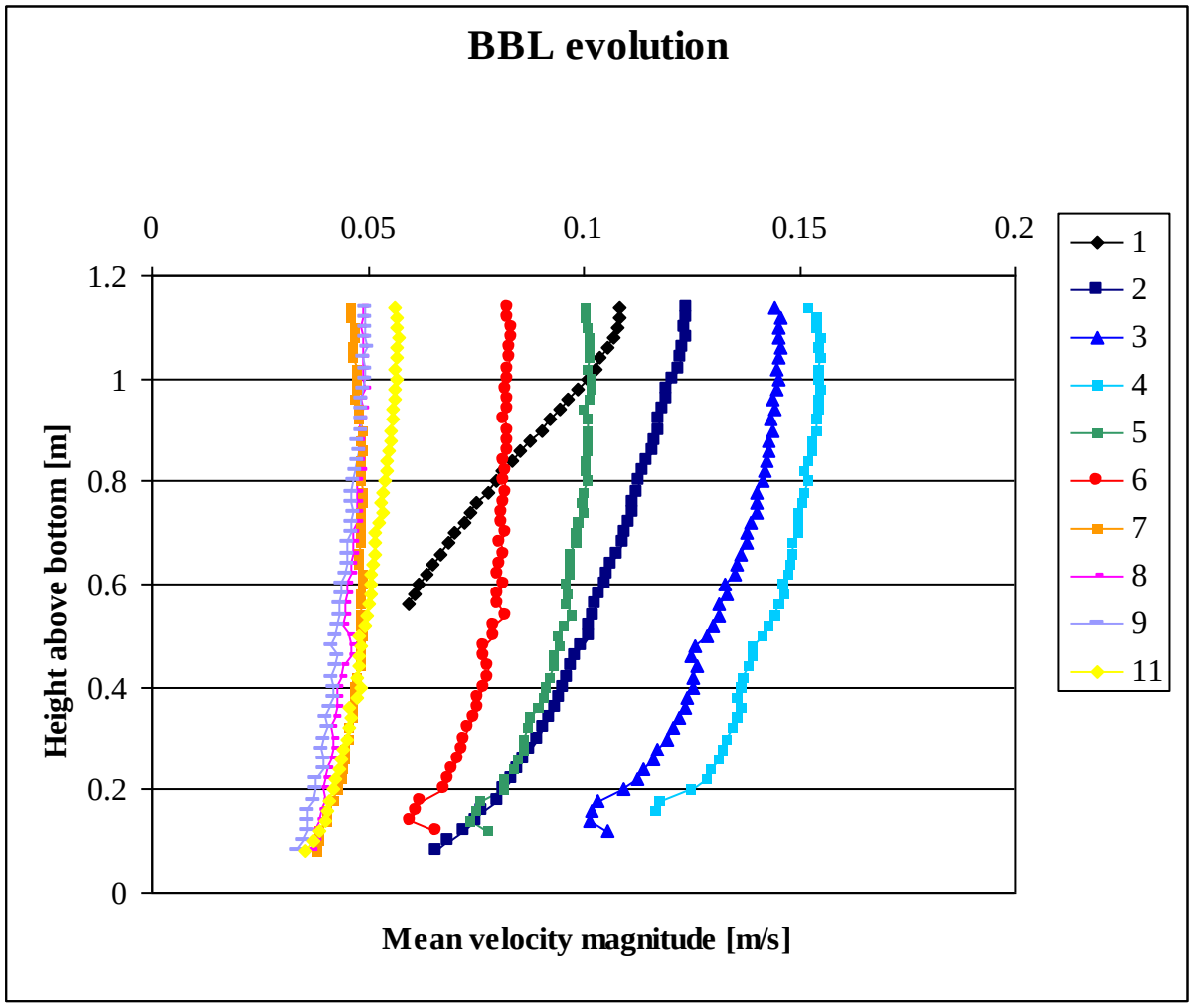

Figure 21. *Bottom boundary layer shape during the deployment. The mean magnitude of velocity changes logarithmically with height above the sea bed. Values from 1-10 indicate the run number corresponding to the operational time of ADVs. (See Figure 5 for times).*

The friction velocity (u_*) (Figure 22) was found to range from 3 to 9mm/s which is consistent with the values previously reported for a flat topography (Chris and Cadwell, 1984). The values of u_* around 1cm/s may suggest that the wave activity was greater during that period (Grant et al.,1984). The energy spectra (Figure 20) showed that the period of waves almost did not change during the whole flood. However, waves of the same frequency could affect the BBL greater during LW because the wave orbital velocities decrease with depth. Furthermore, It was found that bottom roughness and stress decreased with time during the first three hours of deployment (Figure 22). After that, a slight increase can be observed. Bottom shear

reached its maximum, 0.09 Pa, at the start of the deployment (LW). Its minimum, equal to $2*10^{-5}$ Pa, occurred after 3.7 hours from the start of the deployment.

The log-layer method used here to estimate the friction velocity suffers because it can be applied only for a steady flow and measurements must have a good accuracy to provide a high regression coefficient. Also the oceanic boundary layers are more complicated because the velocity vector is rotated with depth due to the Coriolis force. Another difficulty observed in this study is the effect of sea surface waves on BBL. If the swell is strong enough the velocity of orbital motion caused by waves can exceeds the mean flow velocity. This can cause the log layer to be no longer present in the BBL (Nimmo Smith et al., 2001).

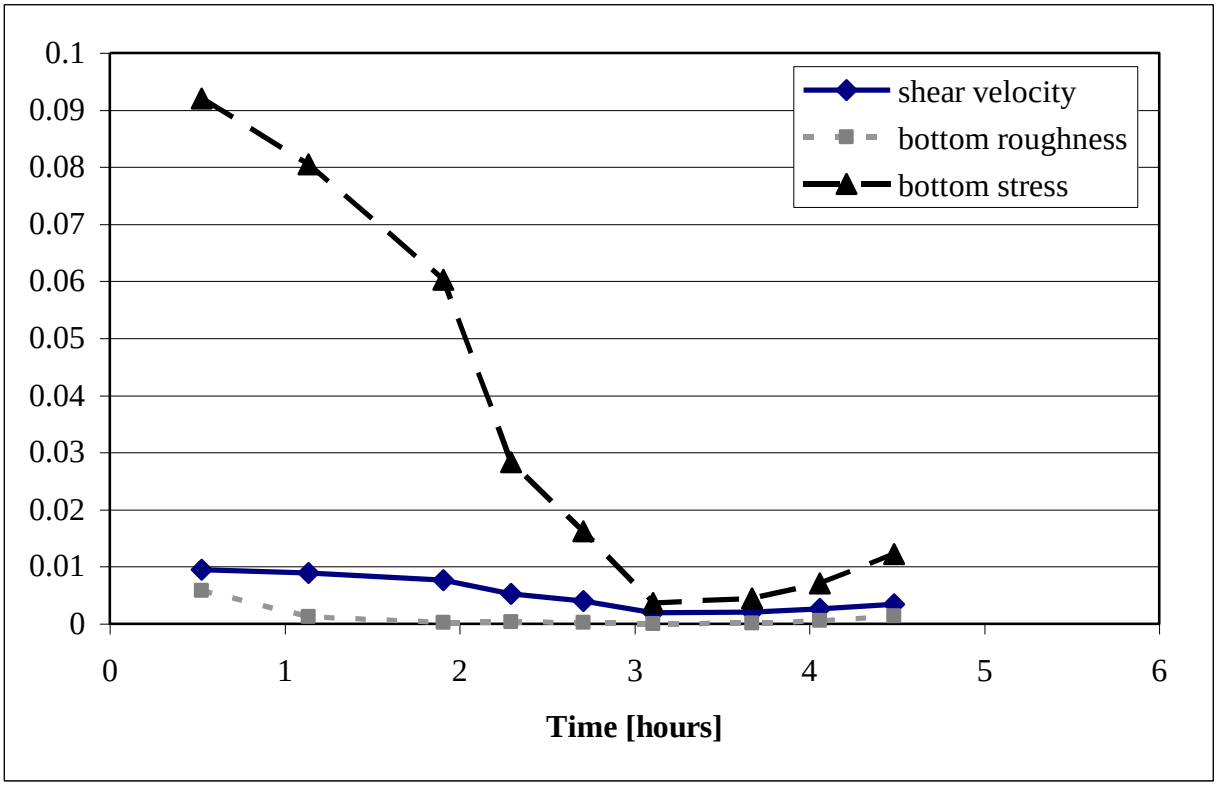

Figure 22. *Time series of friction velocity, bottom roughness and bed stress during the flood tide, calculated from the equation 3 (See section 2.2). The parameters were not calculated for the first run because of its limited range (only 58cm).*

4.4. TKE Dissipation Rate

Time series of dissipation rate (ε), obtained form the two ADVs, are shown in Figures 23 & 24. The purple dots indicate the time when the energy spectrum did not have inertial range or the inertial range was very small. It was found that during few periods of measurement all three velocity components spectra did not have inertial sub-range. These records should not be used for the calculation of dissipation rate because the assumptions of the method did not hold in that case. Furthermore, the vertical velocity spectra calculated for two ADVs did not fit well into the Kolmogorov's model (Figure 25).The slope of the inertial range was found to be less than -5/3 for the vertical component. Generally, the inertial sub-range was not present at the start and the end of the deployment, when the mean and fluctuating velocities were found to be the smallest. An example of a spectrum which did not have inertial part is shown in Figure 26. This spectrum can be divided only into two parts: noise of the instrument (flat part) and large scale fluctuations (waves). The opposite, spectrum with a clear inertial range is shown in Figure 27. It can be seen that the noise frequency ranged here from 6Hz to 11Hz and inertial sub-range occupied almost the rest of the spectrum (0.01Hz - 6 Hz). Waves could bias the estimation of ε if their frequency was similar to the frequency of turbulent eddies. However, this should not happen in this research because the waves' frequency was lower (0.01Hz) than the frequencies corresponding to the energy carrying, turbulent eddies (Figure 27).

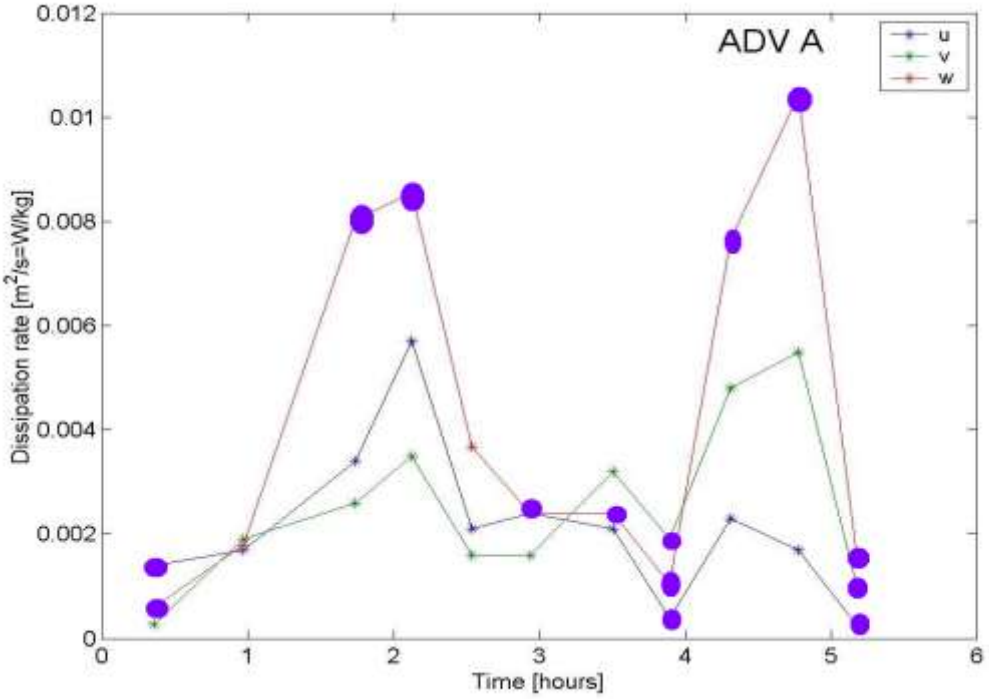

***Figure 23**. Dissipation rate calculated by applying the 'inertial range' method on the ADV A velocity components (horizontal: u, v and vertical: w). Purple dots indicate the places where the spectra did not have inertial sub range.*

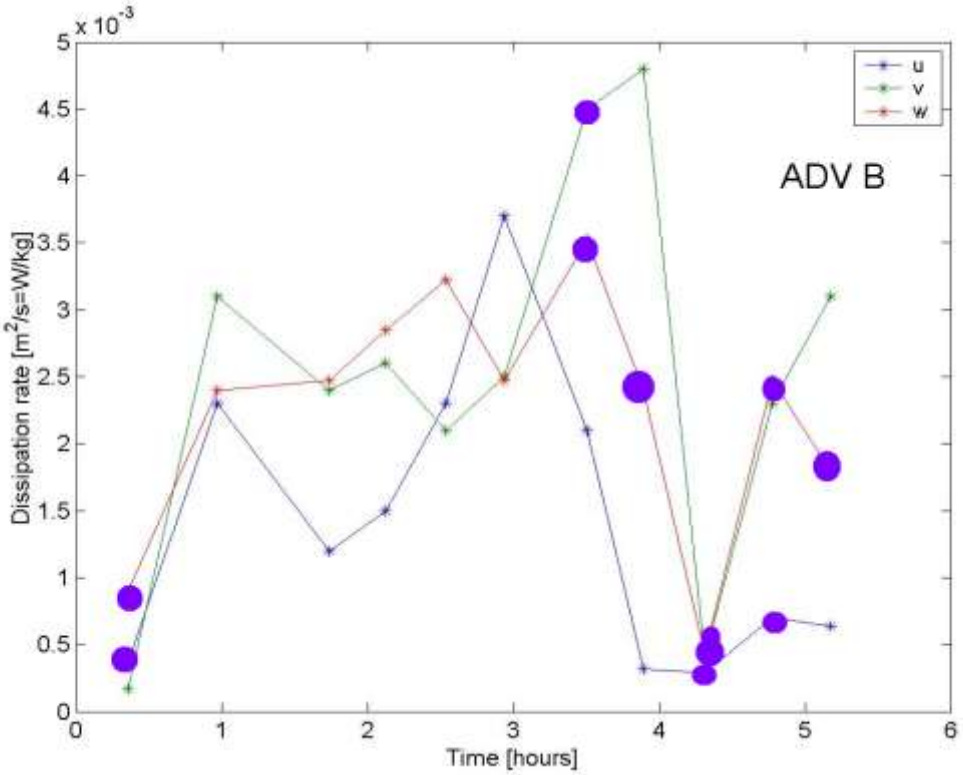

***Figure 24.** Dissipation rate calculated by applying the 'inertial range' method on the ADV B velocity components (horizontal: u, v and vertical: w). Purple dots indicate the places where the spectra did not have inertial sub range.*

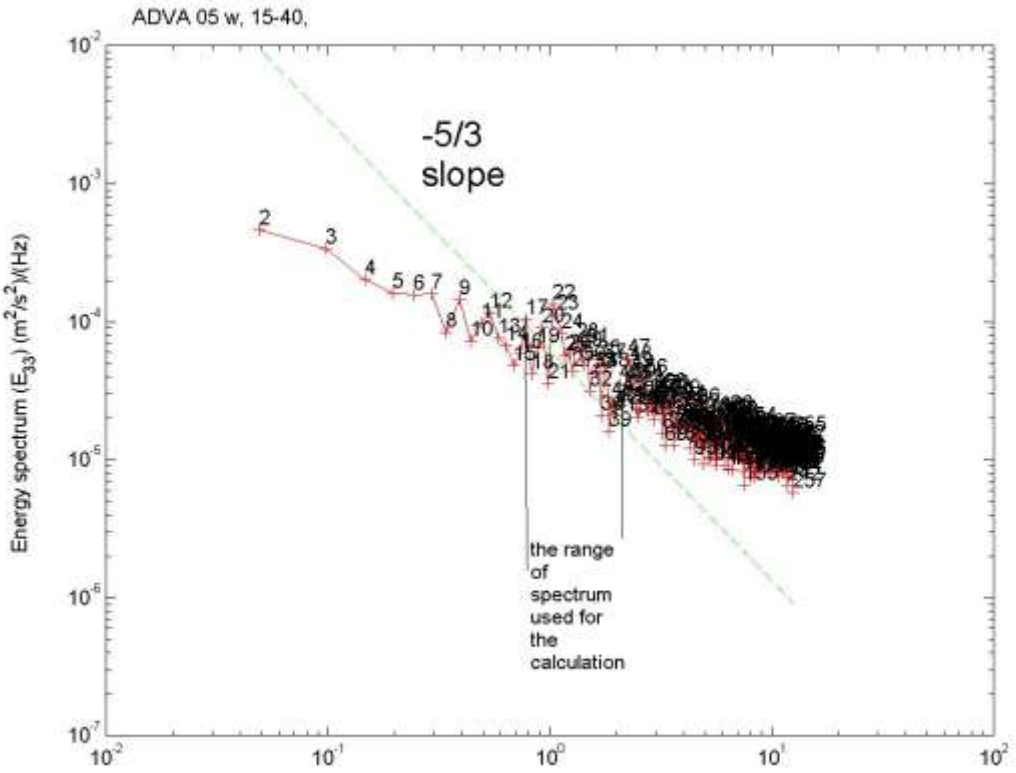

***Figure 25**. A spectrum of the vertical component of velocity vector at run 4. The range used for the calculation of dissipation rate was from 15 to 40 data points. The line of -5/3 slope does not fit well into the data.*

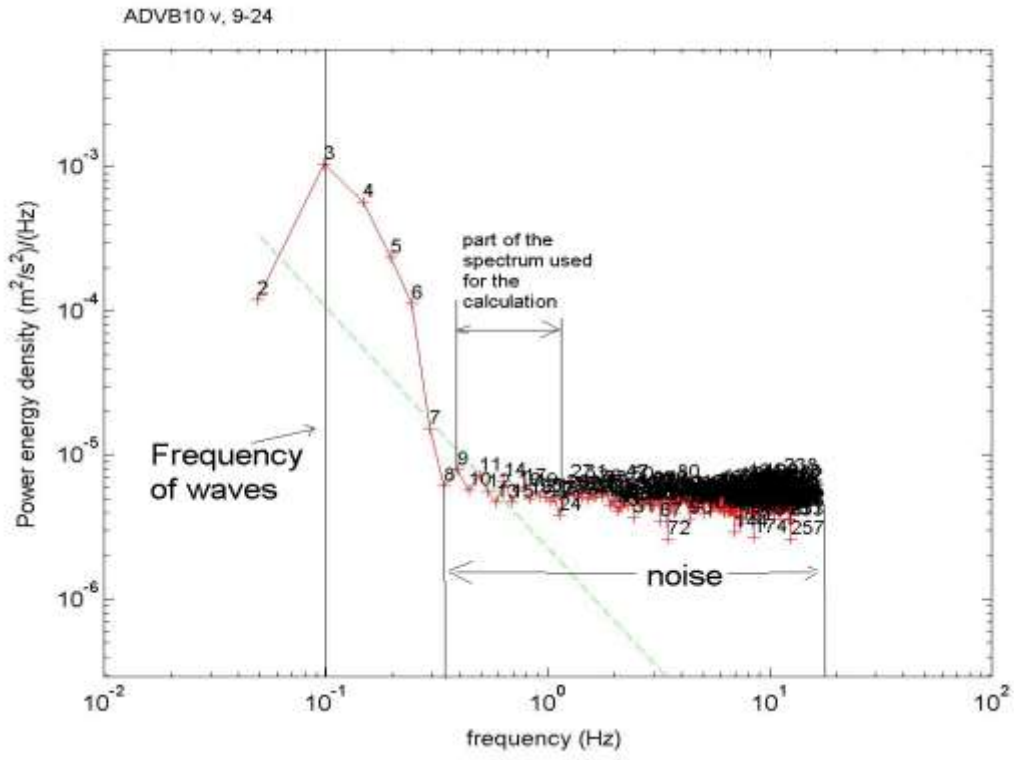

***Figure 26**. A spectrum of cross stream component of velocity vector at run 9. The range used for the calculation of dissipation rate was from 9 to 24 data points. The spectrum has not an inertial range.*

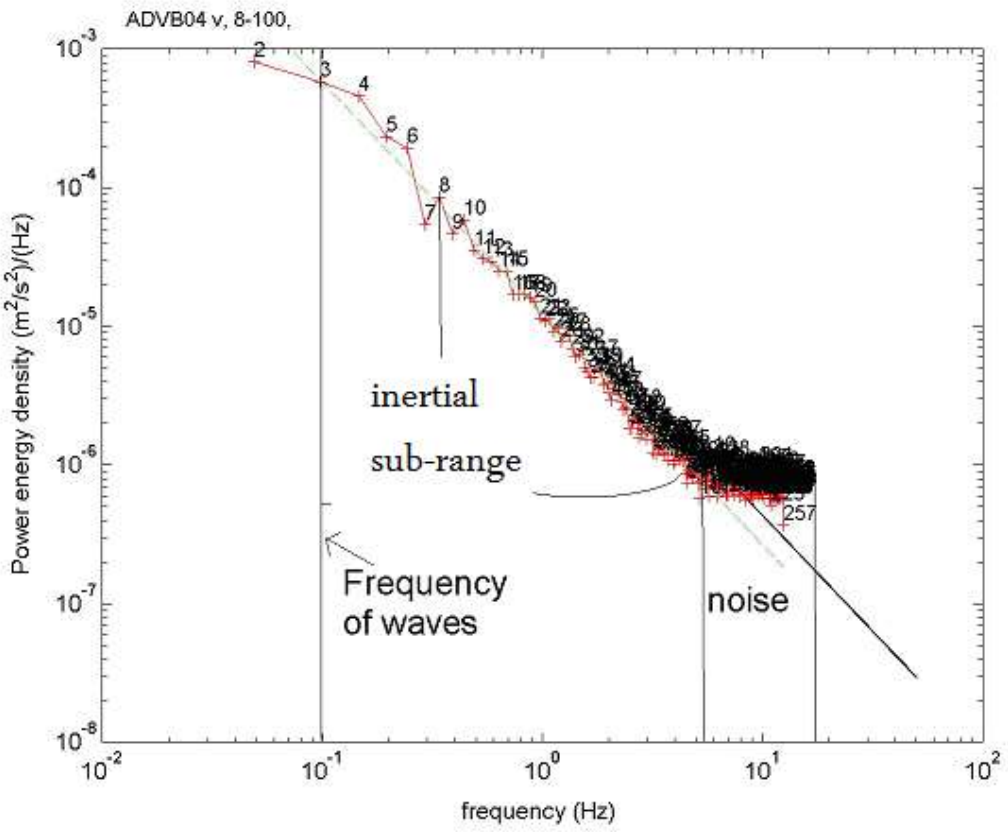

***Figure 27**. A spectrum of cross-stream component of velocity vector at run 3 with clear inertial sub-range. The range used for the calculation of dissipation rate was from 8 to 100 data points.*

It was confirmed by the previous research (Lien & D'Asaro,2004;) that the ADV velocity spectra can resolve ε as low as 10^{-8} W/kg. A comparison of dissipation rates obtained at two elevations (A and B) is shown in Figure 28. It can be observed that dissipation rate obtained at the two depths had similar magnitudes (10^{-3} W/kg) and trends. Dissipation rate increased with velocities and remained at the level of about $3*10^{-3}$W/kg until the end of the flood. However, the results reported here are noisy and the assumptions used in the method for the calculation were not met. The difference in the dissipation rate can be seen between the two techniques: the 'inertial range' method applied to the ADV data (Figure 28) and the 'structure function' method used to process the 1.2MHz ADCP data (Figure 29). The results differ from each other by three levels of magnitude, and ADVs give the higher estimations. However, the comparison of ε estimations between different sensors can be difficult for inhomogeneous turbulence (Moum et al., 1995).

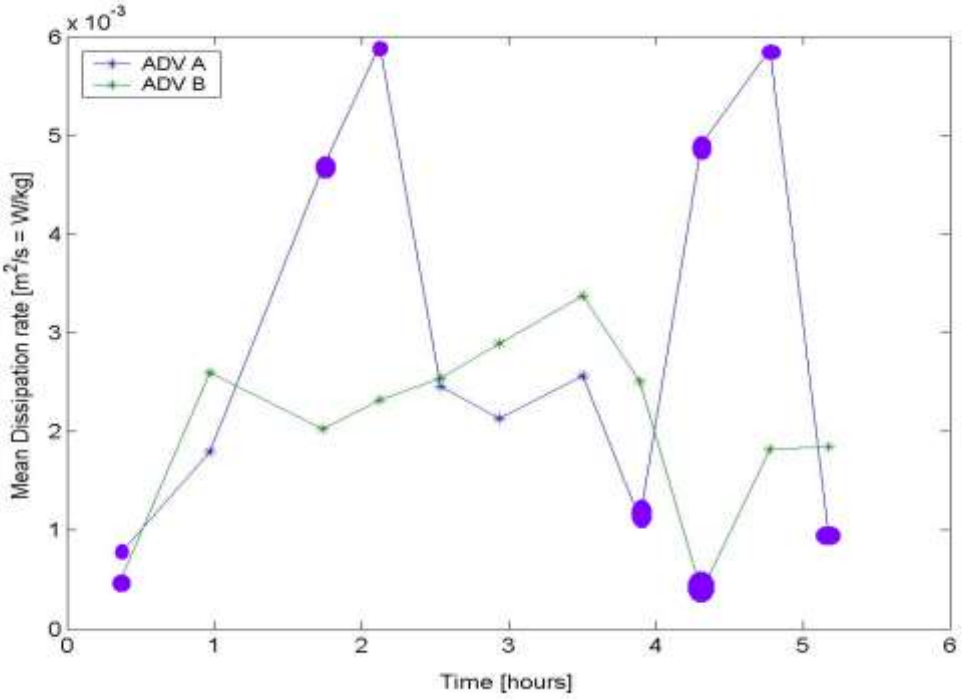

***Figure 28**. Mean dissipation rate obtained by averaging the dissipation from three velocity components. Purple dots indicate the places where the spectra did not have inertial rage.*

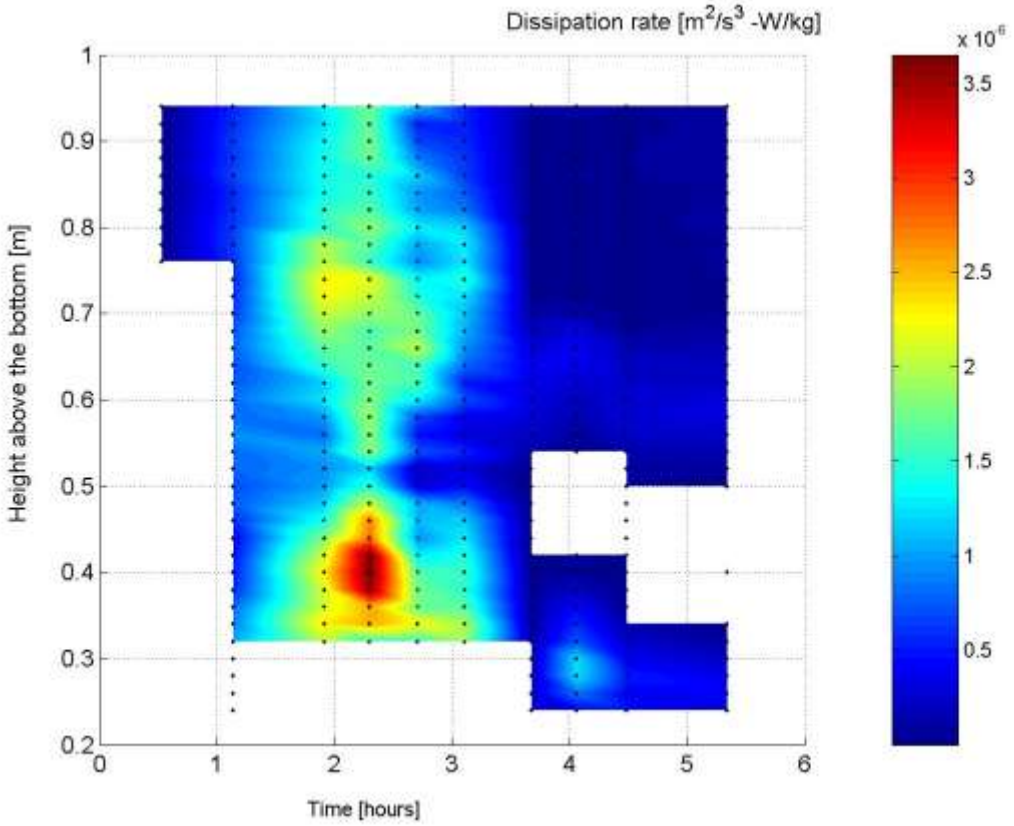

***Figure 29**. Dissipation rate obtained using 'structure function' method on the 1.2MHz ADCP data. Data points are indicated by black dots. Notice the missing data at the right (bottom corner of the picture) due to results below the noise level of the instrument.*

The results of ε estimates from the ADCP (Figure 29) show that the greatest dissipation occurred near the bed during and just after velocity maximum (2-2.3hours). The maximum value of 3.5 $*10^{-6}$ W/kg was reached at the height equal to about 0.4m above sea bed . At the later time the dissipation was much lower: from 10^{-8} -10^{-6} W/kg. Furthermore, it was found that the method can find the dissipation as low as 1.4$*10^{-9}$ W/kg which is a lower threshold than for an ADV. The results less than this level had negative values (below noise threshold) and therefore are shown in Figure 29 as a blank space. The smallest eddies where TKE is dissipated into heat was found to have a size of 0.7mm for ε=3.5E-6 W/kg and 3mm for ε=1.5E-8 W/kg.

The dissipation rate obtained using the 1.2MHz ADCP is consistent with the previous study, confirming that the upstream facing beams give higher estimations of dissipation rate than downstream faced beams (Wiles et al., 2006). The maximum difference between the upstream and downstream beam was found to be the factor of three. Wiles et al. (2006) argue that the disagreement between the beams in ε estimates is a consequence of anisotropy in stress and shear. Therefore, the resulted values of ε reported in this paper were averaged over four beams to provide a more accurate estimation.

Dissipation rate reported by Lorke and Wüest (2005) in the BBL in Lake Alpnach (Switzerland) during low energetic flow (maximum current speed equal to 3cm/s), was calculated using 'inertial range' method to the ADCP data. The dissipation they found was much smaller than reported in this study (10^{-11}-10^{-8} W/kg), which could be expected owing to a much slower flow. It was reported that ε for more energetic tidal flow (Red Warf Bay, maximum velocities during the flood 0.2m/s), estimated by the 'structure function' method using a 1.2MHz ADCP , was found to be around 0.01W/m^{-3} (9$*10^{-6}$ W/kg) during the flood (Wiles et al., 2006). This study found similar values of ε which occurred for the intermediate fast currents. The velocities measured by the two studies had similar magnitude and therefore can be concluded that the 'structure method' used in this study provided more accurate estimation of ε than the 'inertial range' technique. Furthermore, various recent studies (Nimmo Smith, 2005; Rippeth et al., 2003) reported comparable values of ε for similar flow conditions as found in this study using the 'structure function' technique.

Limitations:

The ‘inertial range’ method used in this research for ε estimation has many limitations. Firstly, isotropic and homogenous turbulence was assumed together with presence of an inertial range. The calculated spectra show that this assumption did not hold when the velocities were low (Figure 22).The noise of the ADVs exceeded the energy contained frequency and therefore the method provided inaccurate estimation of ε. The other limitation is that the streamwise velocity spectra are more susceptible to contamination by waves which could cause the overestimation of ε. It is more convenient to remove the wave frequencies before the analysis (by using the method proposed by Trowbridge (1997)) or use the vertical velocity spectra for the estimation. However, in this research vertical spectra did not have an extended inertial range, and the slope of the range did not match the theoretical spectrum (Figure 23). This could be caused by the orientation of the ADV because an ADV provides more accurate measurements in the z direction. However, the z direction during the study specified the horizontal component of velocity (Figure 6). This means that this component had a lower noise level than the vertical. It is therefore recommended to set the orientation of the ADV head vertically to obtain more accurate estimations of vertical velocity spectra.

When using the ‘inertial range’ one must choose the cut-off frequencies that constitutes the upper limit of the inertial range. This cut-off should be large enough to avoid the loss of data and small enough to exclude the noise of the instrument. Therefore, the wrong cut-off could affect the estimation of ε, providing too high or too low an ε value. In this study, the two cut-off frequencies f_1= 0.4Hz ,f_2=0.43Hz provided similar estimations of ε, that are within 10 % of each other (see Figs. 21-23 to find out which range of spectrum were used for the estimation of ε). The smaller differences in the range of 1-5 % were found when increasing the cut-off frequencies towards the noise frequencies. However, the cut-off frequencies were chosen by visual inspection of the spectra which could cause an error in the estimation.

4.5. Reynolds stress and TKE production

Figures 30 and 31 show mean covariance (Reynolds stress) of *u'* and *w'* during the flood tide. The magnitude of the covariance, calculated using ADV data, increased from the value below the noise threshold of the instrument (about 10^{-8} m^2/s^2) at the start of the flood to 8 * 10^{-5} m^2/s^2 during run 6 (3h). Reynolds stress was found to be greater at the higher elevation above the bottom (ADV A) but both ADVs showed the same trends in Reynolds stress changes with time (Figure 30). The 1.2MHz ADCP estimated Reynolds stress in the 1st meter above the bottom (Figure 31). Similar magnitudes were found, comparing to the ADV's results, which ranged from 10^{-6}- 10^{-4} m^2/s^2. Furthermore, the instrument confirmed that the magnitude of $-\overline{u'w'}$ increased during the first 2.5 hours. It can be observed in Fig. 30 that $\overline{u'w'}$ reached the maximum of about 2*10^{-4} m^2/s^2 during runs 4 and 5 (from 2.3 to 2.7 hours). The maximum stress occurred at depths 0.5 to 1m above sea bed. The study found that Reynolds stress in the cross-stream direction (Figure 33) demonstrated the same trend and magnitude as $\overline{u'w'}$ with the maximum values occurring during run 4 (2.3h) 0.3 m above the bottom. High values were observed at 0.6m above the bed during runs 3-6 which could be caused by fish swimming in the sample volume of the ADCP. This could bias *u'* and *w'* toward the higher values and it can be argued that this is one of the limitations of the method used for the calculation of the stresses ('the variance method'). From other side, $\overline{v'w'}$ obtained from ADVs did not show any trend and remained at the same level during the deployment (Figure 32). Figure 32 shows that $\overline{v'w'}$ changed rapidly from the higher value to the lower, in the short period of time indicating noisy results.

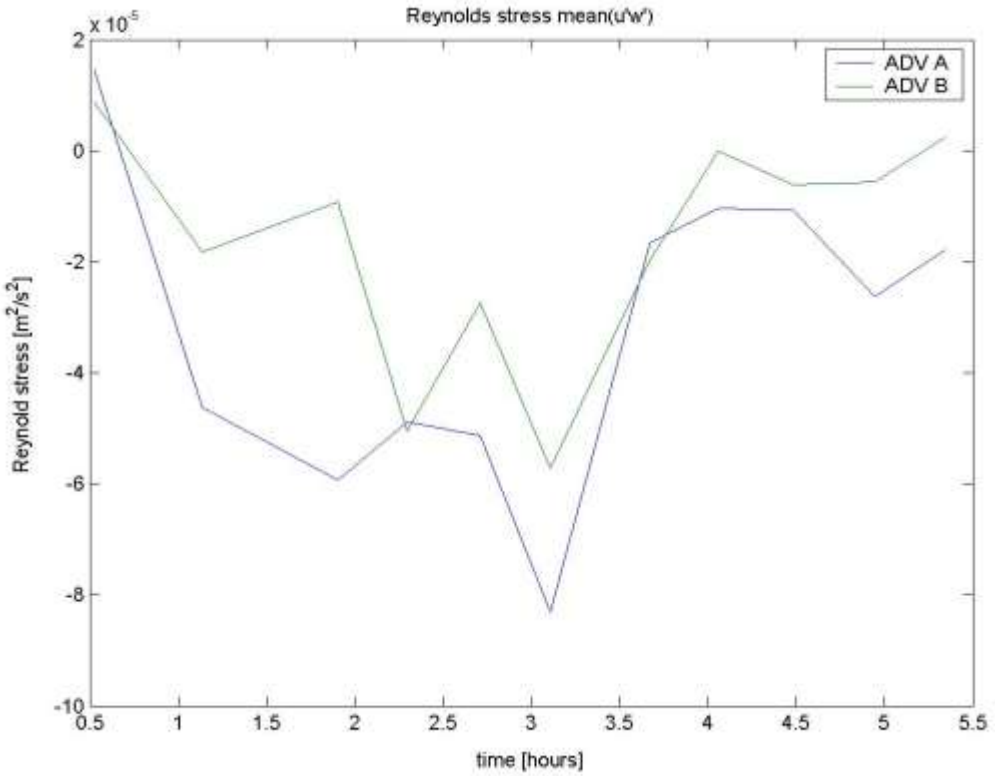

***Figure 30**. Covariance (Reynolds stress/density) of u' and w' (fluctuating velocity components) at two elevations above the bottom.*

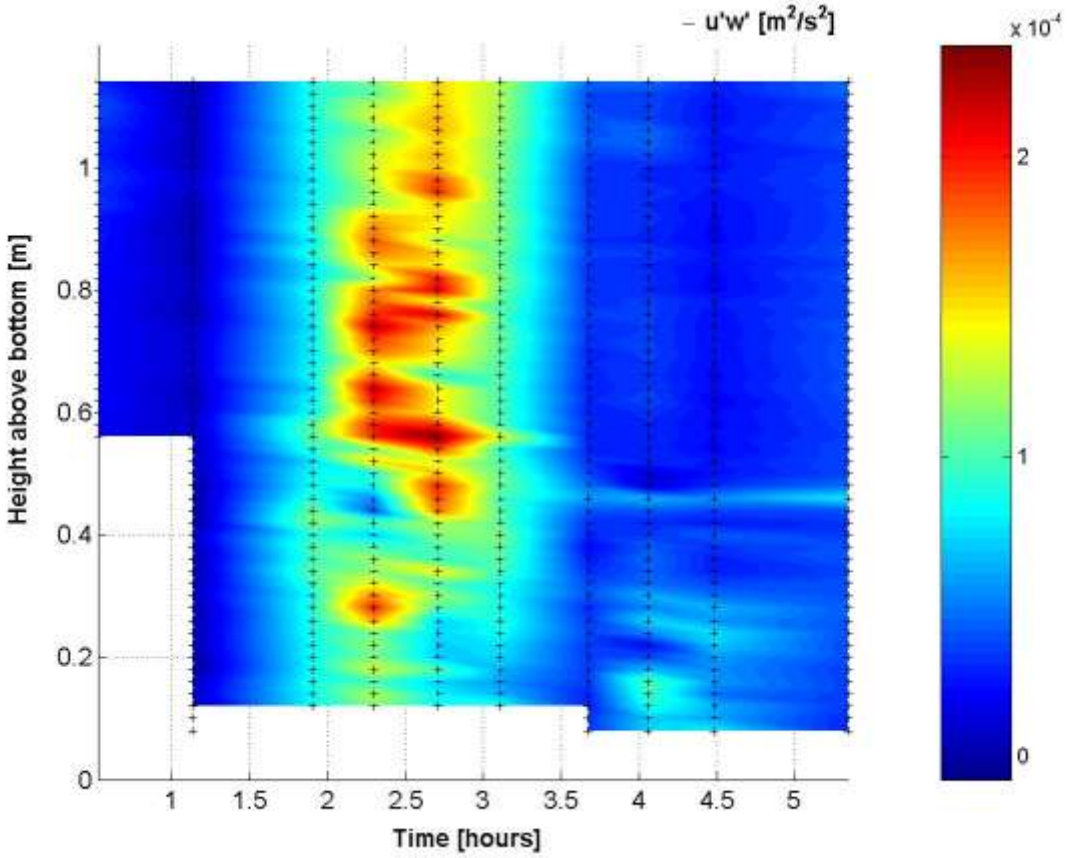

***Figure 31**. Reynolds stress (divided by density) in the streamwise direction calculated from 1.2MHz ADCP measurements.*

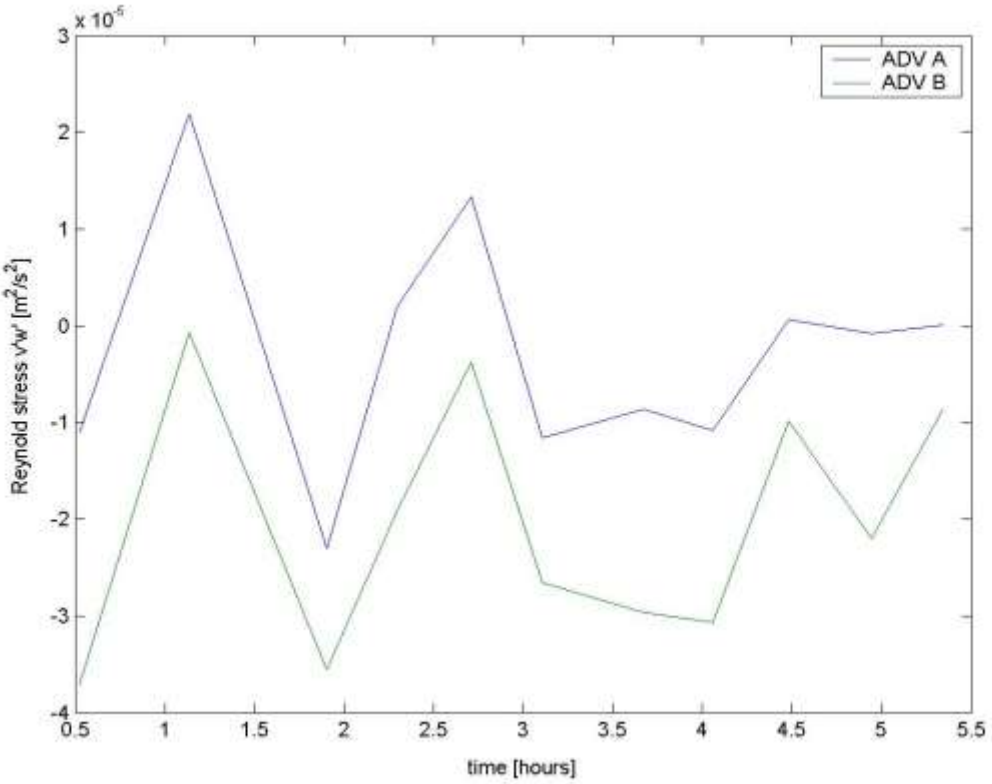

Figure 32. *Covariance (Reynolds stress/density) of the v' and w' fluctuating velocity components at two elevations above the bottom.*

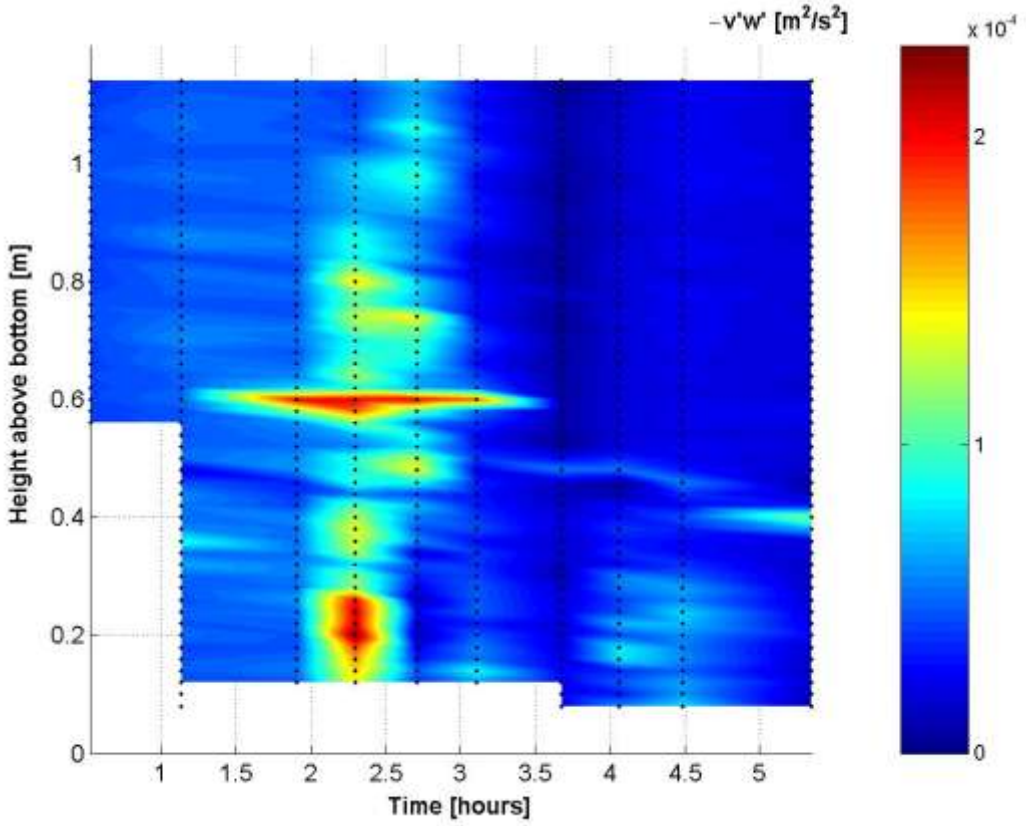

Figure 33.*. Reynolds stress (divided by density) in the cross-streamwise direction calculated from 1.2MHz ADCP measurements.*

The dominant component of stress was found to be $\overline{u'w'}$ and therefore production (P) of TKE was calculated using $\overline{u'w'}$ and stream velocity gradient (or velocity magnitude gradient when considering the ADCP). The production of TKE is shown in Figures 34 and 35. The results show that both instruments measured negative values of production at the start of deployment. It was reported previously (Rippeth et al., 2003) that negative values of P are a result of lack of coherence between the stress and shear estimates due to influence of the noise. Therefore, it can be concluded that the negative values indicated the production bellow the noise threshold of the instruments. It was found that the negative values of P occurred in the same time and elevation that low values of ε (10^{-8} W/kg). The threshold for the P estimates was identified as $2*10^{-9}$ W/kg which is much lower value than previously reported for the 1.2MHz ADCP ($6.8*10^{-8}$ W/kg, Rippeth et al., 2003). The lower noise threshold can be explained by a greater accuracy of the measurements reported here due to the use of a higher accuracy, RDI mode 11.

The study found that TKE production ranged from $1*10^{-8}$- $3*10^{-5}$ W/kg for ADCP and $4.5*10^{-8}$ to $2*10^{-6}$ W/kg for ADVs (Figures 34&35). Both techniques used for the calculation of TKE production are consistent with each other. For example, both show that at the elevation equal to 60cm above sea bed, TKE production had the magnitude of about 10^{-6} W/kg. Figure 35 shows that the greatest production of TKE occurred during run 3-5 (2-3hours) at 20cm above bottom. It could be concluded that the high TKE production values are associated with high velocities near the bed (high shear). The production in the first meter above the bed was highest when the Reynolds stress and shear was the largest, which is consistent with previous studies (Wiles et al., 2006).

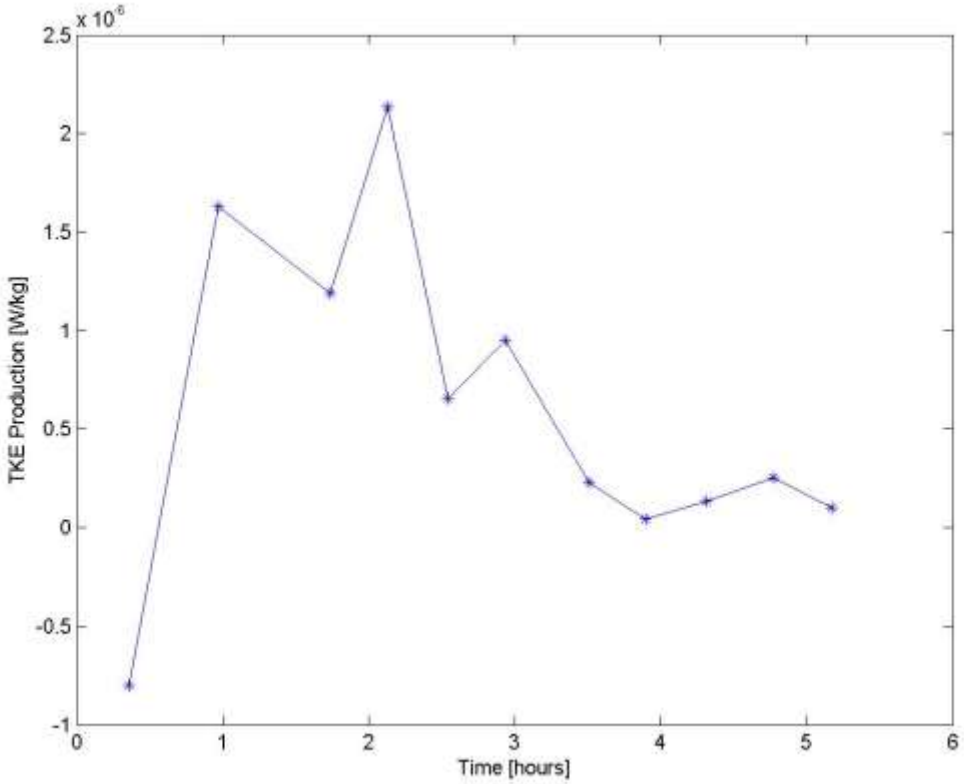

***Figure 34**. TKE Production [W/kg] at 60.5cm above bottom, obtained from two ADVs data.*

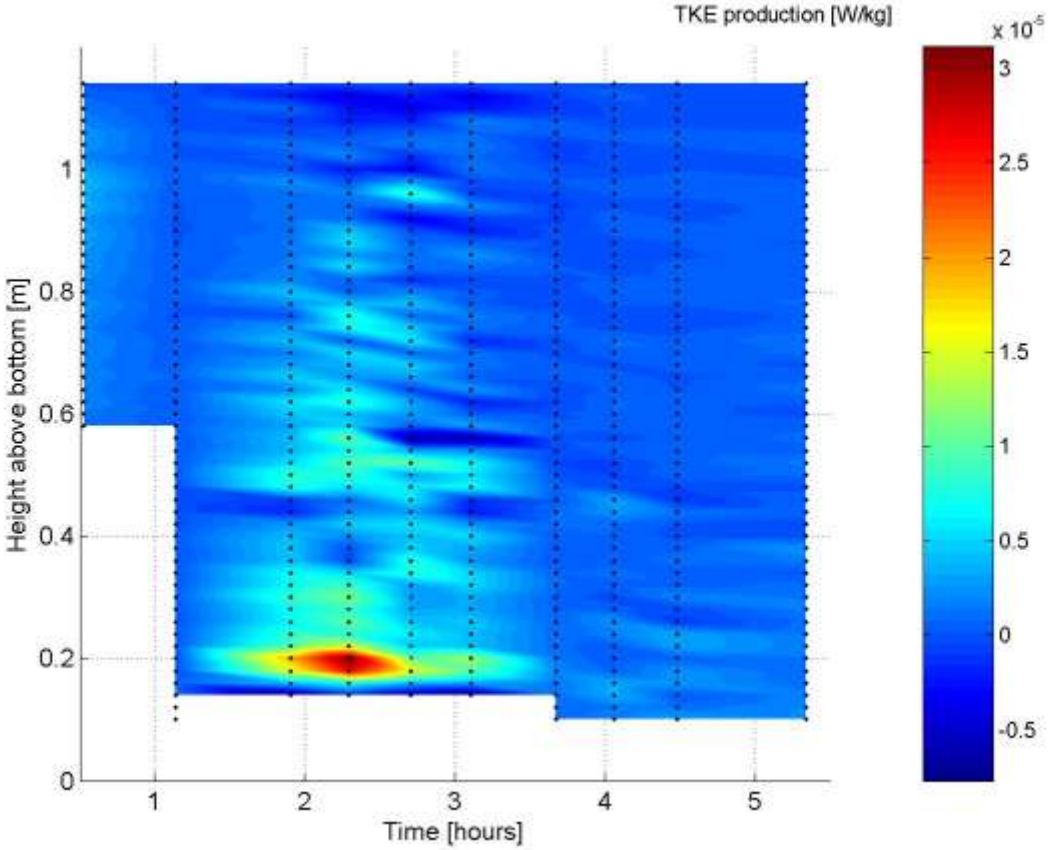

***Figure 35**. TKE production [W/kg] obtained from 1.2MHz ADCP measurements.*

Recent studies proved that ADV sensor can measure mean velocity and Reynolds stress within 1% of the estimated true value (Voulgaris & Trowbridge, 1998). The errors associated with the method were found to be caused by the misalignment angle in the orientation of the instrument and the differences between the velocity variances due to the geometry of the sensor. However, the maximum error was found to be small, around 1.3% for velocity variance, and was estimated in this study to be 0.01cm^2/s^2 . Other studies, which compared the ADCP 'variance method' and ADV direct estimation of Reynolds stress, demonstrated that both methods are consistent with each other and the regression coefficient (R^2) for the methods was found to be 97% (Souza & Howarth, 2005). However, it was reported that during the strong wave activity, the methods did not produce similar results and R^2 was found not to be significant (4%).

The stress calculated using the 'variance method' can be biased due to a combination of instrument tilt and surface wave activity. The tilt of about 2^0 can cause a significant bias (Rippeth et al., 2003) because the Reynolds stress is proportional to the magnitude of the tilt angles (Lohrmann et al., 1990). For example, the roll angle equal to 0.5^0 will bias the estimation less than 1% for $\overline{u'w'}$ and 6% for $\overline{v'w'}$ (Rippeth et al., 2003). In this study the magnitude of roll angle of the ADCP ranged from 0.04^0 during run 10 and 0.74^0 during run 2, causing the maximum error less than 1.5% for $\overline{u'w'}$ and 8.9% for $\overline{v'w'}$. The pitch angle of the ADCP can bias the estimation with little significance for isotropic turbulence (Lohrmann et. A., 1990). However, the pitch could bias significantly the reported results strongly if anisotropic turbulence occurred. It was estimated by Lu and Lueck (1999) that the pitch could contribute 8.5% per degree to Reynolds stress estimation. In this study the maximum pitch was found to be -2.57^0 which could result in an overestimation in $\overline{u'w'}$ and $\overline{v'w'}$ by 21% and 4% (assuming fully anisotropic turbulence). It was found that the value of pitch was around 2^0 during runs: 3-6 but was below 1^0 during most of the deployment time. Surface waves could also bias the estimation of Reynolds stress from the ADV and the ADCP. It is recommended to check the magnitude of the bias which can be estimated by the linear intermediate wave equations (Rippeth et al., 2003). However, the bias in the Reynolds stress estimation due to waves was found to be small near the bed (Rippeth et al. , 2003). The bias in $\overline{u'w'}$ could result in an

overestimate in the Reynolds stress reported in this study. The total error in the results is a product of wave bias multiplied by the pitch bias and the roll bias (less than 25%).

4.6 Comparison of P and ε

Figures 36 & 37 show P and ε in the logarithmic scale. The results obtained from the 1.2MHz ADCP indicate that the rate of TKE production had the same magnitude as the dissipation rate. The comparison between P and ε was performed by calculating individual ratios of P corresponding to ε . In this calculation the values of P which were unreliable (negative) were not used. The study found that the ratio ε/P averaged over whole flood was equal to 1.45 +/- 1.07 indicating that the dissipation exceeded the production. The reported ratio has a significant deviation from the expected, theoretical value of unity. However, when considering each period of measurement separately, it was found that the ratio greater than one occurred only during the start and at the end of deployment that biased the total ratio towards larger values. The 2^{nd} run biased greatly that ratio and causing a big standard deviation in the resultant ε/P estimation. Rejecting that run caused ε/P to be 0.78 +/- 0.36 which is very close to the expected value of unity. It can be argued that the dissipation exceeded production at the slack water, whereas the production was greater when the flow accelerated.

Previous studies also showed a deviation of ε/P ratio from unity which was much greater than reported here (Lu et al., 2000, Rippeth et al., 2003). The question arising from the reported results: What happen during run 2 which resulted in much greater estimations of ε than of P? It can be argued that the flood mean ε/P> 1 could be caused by errors associated with the methods used in this research to estimate both parameters. However, that could also be caused by other terms present in the TKE equation (equation 3). For example, convection by the mean flow and advection by fluctuating velocities could cause the transfer of TKE energy from and out the sampling volumes of the instruments.

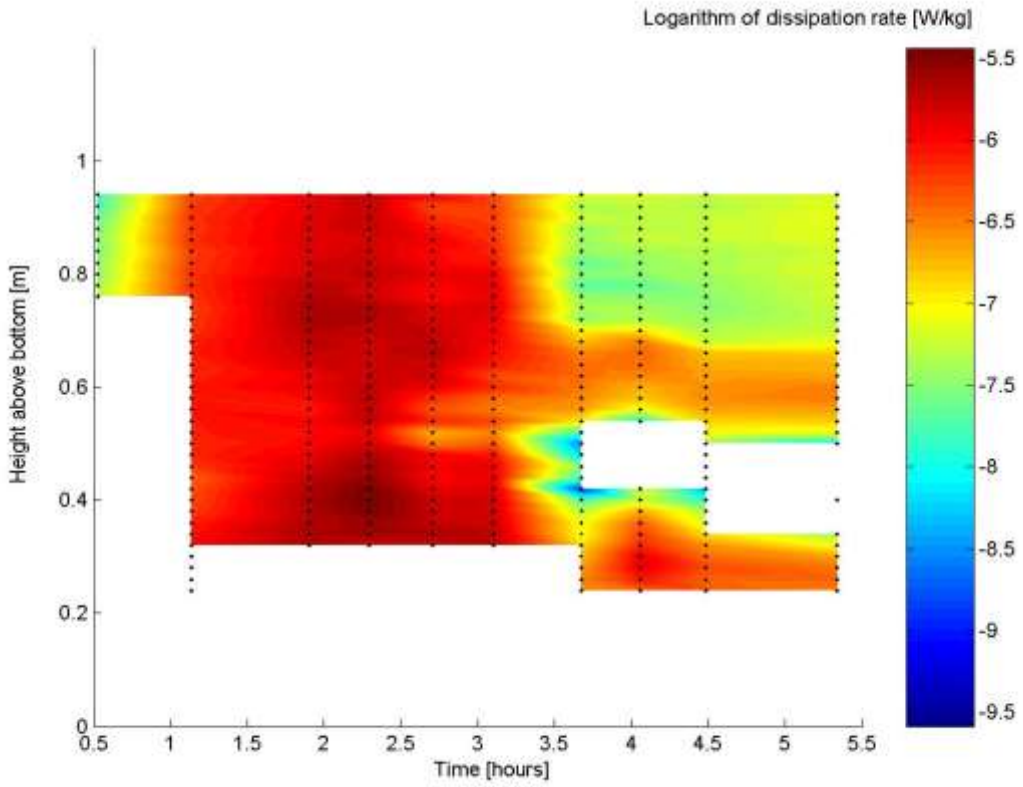

Figure 36. *Dissipation rate showed in logarithmic scale [W/kg].*

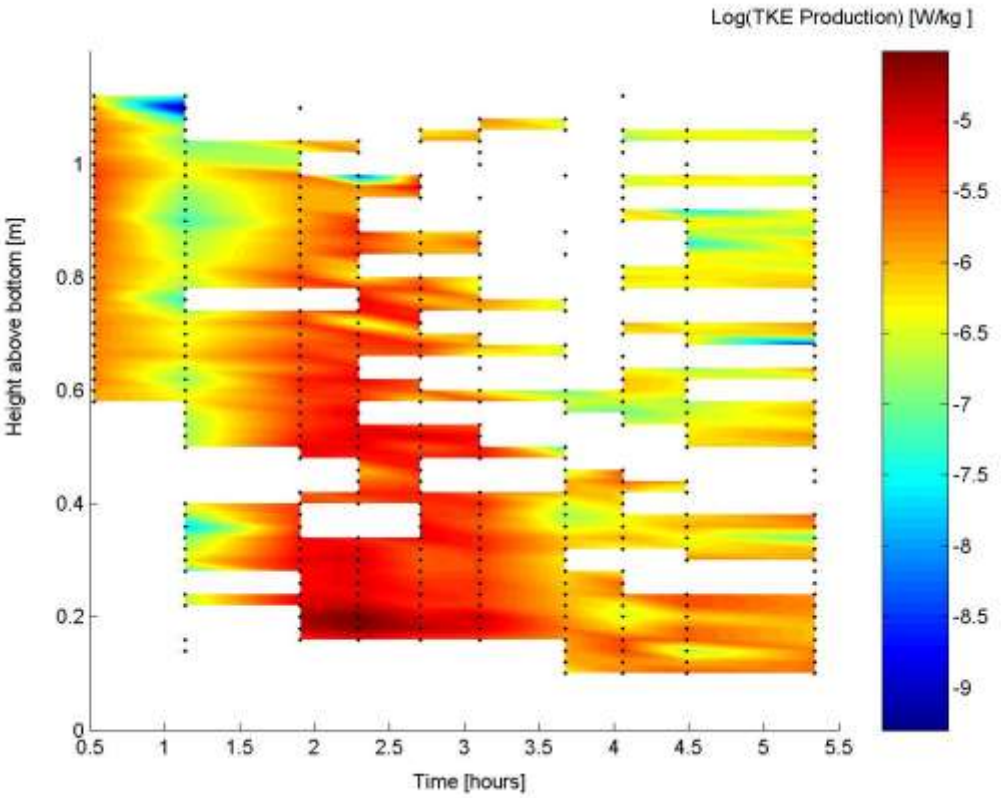

Figure 37. *TKE production rate in the logarithmic scale [W/kg].The blank places indicate where P was less that the instrument noise.*

It is recommended to examine whether the assumptions, applied to the two methods of estimation of ε and P, held during the deployment further. For example, Stacey et al. (1999) proposed a method for examining the assumption about temporal stationarity of the flow and velocity variances using an ADCP. Additional bias in the ADCP measurements may be due to its vertical resolution. The greater the bin size the greater the error in the velocity fluctuation caused by the ADCP spatial averaging within its bins. However, in this study the bin size of 2 cm was used, which means that only very small eddies were unresolved by the ADCP. Therefore, the bias in the Reynolds stress and P should be small. Furthermore, the assumption of the spatial homogeneity of the flow applied to the calculation of P and could not be true ε because the assumption requires that the opposite beams sample the turbulence which has the same statistics. In this research the maximum beam spread of 1.2MHz ADCP was 0.93^0 and therefore the required homogeneity for the calculations could be assumed. Recent research (Stacey et al., 1999) confirmed that the estimation of Reynolds stress is not affected by the Doppler noise. However, the noise could affect ε estimations (Wiles et al., 2006). Also the variations reported in section 4.4 between ε calculation using upstream and downstream beams could bias the estimation.

5. CONCLUSIONS

The study have found that the density stratification did not affect turbulence in the BBL what confirms Richardson number less than 0.25 during the most time of deployment. Therefore, it can be concluded that the shear instabilities generated by the tide gave rise to turbulent mixing that caused the water column to be unstratified during the flood phase of tide. The flow was a result of semidiurnal tide with maximum velocities observed during first three hours of the flood at 4m above the bed. During that time there was a lot of shear production and the direction of the flow varied from 220^0 in the top 6m of the water column to 60^0 in the 4m next to the sea bed. The velocities measured by two ADVs and the 1.2MHz ADCP were found to be consistent with each other, showing the same trends and magnitude of flow.

The velocities in the first meter above sea bed were measured by the 1.2MHz ADCP. The results show that the mean velocity had a logarithmic profile in that layer that allowed a calculation of the time series of shear velocity, bottom roughness and bed stress. The results were found to be consistent with previous studies reported for the flat topography. The largest values observed at the LW indicate a greater effect of waves on the turbulent parameters. The rate of TKE dissipation was estimated by applying 'inertial range' technique to the ADV data and 'second order structure' to the 1.2 MHz ADCP data. The study found 'inertial range' method to be not accurate and producing three orders of magnitude higher results then the other method. Furthermore, a comparison with recent studies, reported for similar conditions, show that the ADV overestimated ε greatly. This discrepancy was caused because the assumption of the 'inertial range' method did not hold what caused the method to be useless in that case. The dissipation was found to be the greatest ($3.5*10^{-6}$W/kg) near to the bed, when the fastest flow occurred. Furthermore, it was found that the 1.2MHz ADCP can resolve ε as low as $1.4*10^{-9}$ W/kg, which is a lower threshold than found for an ADV.

Reynolds stress was estimated directly from the ADV and by using the 'variance technique' on the 1.2MHz ADCP velocity measurements. The two devices provided similar results (10^{-5}-10^{-4} m^2/s^2). It was found that the Reynolds stress ranged from 10^{-6}-10^{-4} m^2/s^2 and the greatest values were observed during runs 4 and 5. The

dominant stress was the streamwise component of velocity, which was used for the calculation of TKE production rate. The production was found to be negative below $2*10^{-9}$ W/kg and ranged from $1*10^{-8}$ to $3*10^{-5}$ W/kg for ADCP, and $4.5*10^{-8}$ to $2*10^{-6}$ W/kg for ADVs. Both techniques used in this study for the estimation of P were found to be consistent with each other. The comparison between P and ε was performed by calculating individual ratios of P corresponding to ε. The study found that the ratio ε/P averaged over whole flood was equal to 1.45 +/- 1.07, indicating that dissipation exceeded the production. However, during different runs different characteristics dominated in the TKE balance. For example, dissipation exceeded production at the slack water, whereas the production was greater when the flow accelerated. It was found that the greatest difference between ε and P occurred during run 2 and significantly biased the mean flood ε/P ratio towards more than unity. Rejecting run 2 caused the mean ratio to be much closer to unity and reduced its spread (0.78+/- 0.36). It can be argued that the flood mean ε/P ratio different than one could be caused by errors associated with the methods used in this research for ε and P estimation. However, that could also be caused by TKE convection by the mean flow of an advection of TKE by fluctuating velocity. Therefore, it is recommended to examine various limitations of the methods and analyse the errors associated with them.

6. REFERENCES

Boldyrev S. (2007) “Kolomogrov Turbulence”. *Lecture Notes*, University of Chicago, reviewed on 03.02.2007 from:
http://cmpd.physics.ucla.edu/2007_lectures_homework/boldyrevneutfluidturblec.pdf

Bradshaw P. (1971), *An introduction to turbulence and its measurement.* Pergamon Press, Oxford.

Cacchione D.A, Drake D.E., (1990), *Shelf sediment transport: An overview with applications to the Northern California continental shelf*. , Chapter 21.

Cacchione D.A, Drake D.E., Tate G.B., Ferreira J.T., (1994)”Bottom stress estimates and sand transport on the northern California inner continental shelf” *American Geophysical Union*, **75**, 181.

Chriss T.M., Cadwell D.R., (1984) “Universal similarity and the thickness of the viscous sublayer at the ocean floor.” Journal of Geophysical Research, 6403-6414.

Dyer K.R (1997), *Estuaries. A physical introduction.* 2nd ed. John Wiley & Sons Ltd.

Garcia C.M., Cantero M.I, Nino Y.,Garcia M.H (2004) “Acoustic Doppler Velocimeters Performance Curves sampling the flow Turbulence”, *04 World Water & Environmental Resources Congress*, ASCE, Utah

Garret A.E., (1994),”Observing turbulence with a modified Acoustic Doppler Current Profiler.” J*ournal of Atmospheric and Oceanic Technology,* **11**, pp.1592-1610.

Gordon R.L. (1996) *Acoustic Doppler Current Profiler: Principles of Operation. A practical Primer.* RD Instruments, California.

Grant W.D., Williams A.J., Glenn S.M. (1984),”Bottom stress estimates and their prediction on the Northern California Continental Shelf during CODE-1.”*Journal of Physical Oceanography*,**14**, 506-527.

Johanes Keppler University, Institute of Fluid Mechanics and Heat Transfer, Acoustic Doppler Velocimeter, Linz , reviewed on 20.03.2007 from:
http://fluid.jku.at/hp/images/stories/research/adv.gif

Kim, S.C., Friedrichs, C.T., Maa, J.P.Y., Wright, L.D., (2000). “Estimating bottom stress in tidal boundary layer from acoustic Doppler Velocimeter data”. *Journal of Hydraulic Engineering* ,**126** (6), 399–406.

Laufer J., (1954), “The Structure of Turbulence in Fully Developed Pipe Flow”, NACA, report no. 1033.

Lien R., D'Asaro E.A. (2006) “Measurement of turbulent kinetic energy dissipation rate with a Lagrangian float” J*ournal of Atmospheric and Oceanic Technology*, 23,7, 964-976.

Lohrmann A., Hackett B., Røed L.P, (1990),“High resolution measurements of turbulence, velocity and stress using pulse-to-pulse coherent sonar.” *Journal of Atmospheric and Oceanic Technology*,**7**,19-37.

Lorke A., Wüest A. (2005) “Application of coherent ADCP for turbulence measurements in the bottom boundary layer”, *Journal of Atmospheric and Oceanic Technology,* **22**, pp: 1821-1828.

Lu Y., Lueck R.G., (1999)”Using a broadband ADCP in a tidal channel: Part I: Mean flow and shear.” J*ournal of Atmospheric and Oceanic Technology*, **16,** 1556-1567.

Lu Y., Lueck R.G, Huang D., (2000),”Turbulence characteristics in a tidal channel.” Journal of Physical Oceanography, 30, 855-867.

Mathieu J., Scott J. (2000), *An introduction to turbulent flow*, Cambridge University Press, New York.

McCave I.N. (2005) “Deposition from Suspension”, *Encyclopaedia of Geology*: *Sedimentary Processes*, (eds. Selly R.C., Cocks L.R.M., Malone J.M.) Oxford, **5**, pp 8-17.

McDonough J.M, (2004) *Introductory lectures on turbulence*. Departments of Mechanical Engineering and Mathematics, University of Kentucky.

Moum J.N.,Greg M.C., Lien R.C., Carr M.E., (1995) ”Comparison of turbulent kinetic energy dissipation rate estimates from two ocean microstructure profilers.” J*ournal of Atmospheric and Oceanic Technology*, **12,** 346-366.

Nimmo Smith W.A.M, Atsavapranee P., Zhu W., Luznik L., Baldwin D.R., Katz J., Osborn T.R. (2001), *PIV measurements in the bottom boundary layer of the coastal ocean*, 4th International Symposium on Particle Image Velocimetry, Gottingen, Germany.

Nimmo Smith W.A.M, Katz J., (2005),”On the structure of turbulence in the bottom boundary layer of the coastal ocean.” *Journal of Physical Oceanography*, **35,** 72-93.

Plimpton, P. E.,Freitag H.P., McPhaden M.J., (1995) “Correcting moored ADCP data for fish-bias errors at 0°, 110°W and 0°, 140°W from 1990 to 1993”, p. 49. *NOAA*, Washington DC.

Plimpton E.P., Freitag H.P, McPhaden M.J. (1999), “ADCP Velocity Errors from Pelagic Fish Schooling around Equatorial Moorings”, *Journal of Atmospheric and Oceanic Technology*, pp. 1212–1223.

Pond S., Pickard G.L., (2005), *Introductory Dynamical Oceanography*. 2nd ed., Pergamon Press.

Pope S.B. (2000), *Turbulent Flows*.1st ed. Cambridge University Press

RD Instruments (2002)" High Resolution Water Profiling Mode 11" *Application Note*

Rippeth T.P., Simpson J.H., Williams E. (2003), "Measurement of the rate of production and dissipation of turbulent kinetic energy in an energetic tidal flow: Red Wharf Bay revisited." *Journal of Physical Oceanography*, **33**, 1889 – 1901.

Rothschild B.J., Osborn T.R. (1988) "Small-scale turbulence and plankton contacts rates", *Journal of Plankton Research*, **10**, pp.465-474.

Sauvageot H. (1992), *Radar Meteorology,* Artech House, Norwood.

Schlichting, H. (1968), *Boundary-Layer Theory*, 6th ed. McGraw-Hill Book Co. New York.

Simpson J.H., Williams E., Brasseur L.H., Brubaker J.M., (2005). "The impact of tidal straining on the cycle of turbulence in a partially stratified estuary." *Continental Shelf Research*, **25**, 51-64.

Souza A.J., Howarth M.J. (2005),"Estimates of Reynolds stress in a highly energetic shelf sea", *Ocean Dynamics*, **55**, pp.490-498.

Stacey M.T., Monismith S.G., Burau J.R. (1999), "Measurements of Reynolds stress profiles in unstratified tidal flow." *Journal of Geophysical Research,* **104**, 10,933-10,949.

Stiansed J.E, Sundby S. (2001),"Improved methods for generating and estimating turbulence in tanks suitable for fish larvae experiments" *Scienta Marina*, **65**(2), pp.151-167.

Sylaiosa G., Boxallb S.R., (1998), "Residual Currents and Flux Estimates in a Partially Mixed Estuary" *Estuarine, Coastal and Shelf Science,* **46**, 671–682.

Taylor, G.I., (1931), 'Effects of variation in density on the stability of superimposed streams of fluids', *Proc. R. Soc. (London), Ser. A*, **132**, 499-523.

Tennkes H. (1975) "Eulerian and Lagrangian time microscales in isotropic turbulence." *Journal of Fluid Mechanics*, **67**, pp.561-567.

Tennekes H., Lumley J.L, (1974), *A first course in turbulence*. The MIT Press, 3rd ed., Cambridge.

Trowbridge J.H. (1998), "On a technique of turbulent shear stress in the presence of surface waves." *Journal of Atmospheric and Oceanic Technology*, **15,** 290-298.

Voulgaris G., Towbridge J.H. (1998),"Evaluation of Acoustic Doppler Velocimeter (ADV) for turbulence measurements", *Journal of Atmospheric and Oceanic Technology,* **15**, pp: 272-288.

Wiles P.J., Rippeth T.P., Simpson J.H., Hendrics P.J. (2006),"A novel technique for measuring the rate of turbulent dissipation in the marine environment" Geophysical Research Letters, **33**, L21608.

Williams, E., and J. H. Simpson, (2004) "Uncertainties in estimates of Reynolds stress and TKE production rate using the ADCP variance method." J*ournal of Atmospheric and Oceanic Technology*, **21,** 347–357.